

AFIT/GAP/ENP/93D-07

AD-A273 774



**S** DTIC  
ELECTE  
DEC 16 1993  
**A**

SHOCK WAVE INTERACTION  
WITH L-SHAPED STRUCTURES

THESIS

Richard C. Miller, Captain, USAF

AFIT/GAP/ENP/93D-07

*93-30489*  
*93-30489*

**93-30489**



Approved for public release; distribution unlimited

**93 12 151 07**

**SHOCK WAVE INTERACTION  
WITH L-SHAPED STRUCTURES**

**THESIS**

**Presented to the Faculty of the Graduate School of Engineering**

**of the Air Force Institute of Technology**

**Air Education and Training Command**

**In Partial Fulfillment of the**

**Requirements for the Degree of**

**Master of Science in Nuclear Engineering**

**Richard C. Miller, B.S.ChE, M.S.**

**Captain, USAF**

**December, 1993**

Accession For	
NTIS CRA&I	<input checked="" type="checkbox"/>
DTIC TAB	<input type="checkbox"/>
Unannounced	<input type="checkbox"/>
Justification	
By	
Distribution/	
Availability Codes	
Dist	Avail and/or Special
A-1	

## *Preface*

The purpose of this study was to investigate the interaction of shock waves with L-shaped buildings: however, an underlying purpose was to examine the potential of Sandia National Laboratories' CTH hydrodynamics code. Although CTH is a very capable code, many questions needed to be answered: "Could we model a realistic shock wave?", "How could we best extract the data we wanted out of the megabytes of data produced?", and "How could we build models that would be efficient enough to run in a workstation environment but still give good resolution?" were three questions that had begun to be answered by Captain John Loftis and Captain Grant Fondaw, both from class GNE93M. Their work and the expertise of my advisor, Dr. Kirk Mathews, provided the springboard for my investigation. I would also like to thank Dr. Gene Hertel and his CTH development team at Sandia National Laboratories for creating and supporting a very powerful computational tool, and the Defense Nuclear Agency for providing Cray computer access. Finally, I thank my family: Camille, Karma, and Bucky, for their unwavering support.

Richard C. Miller

## *Table of Contents*

Preface . . . . .	ii
List of Figures . . . . .	v
List of Tables . . . . .	vii
Abstract . . . . .	viii
I. Introduction . . . . .	1
Background . . . . .	1
Problem and Scope . . . . .	2
Approach . . . . .	3
II. Theory . . . . .	9
CTH's Computational Process . . . . .	9
CTH Code Modules . . . . .	10
CTH's Iterative Three Stage Computational Loop . . . . .	12
Ideal Blast Wave . . . . .	17
Blast Wave Reflections . . . . .	19
Horizontal Loading of Structures . . . . .	22
III. Investigation . . . . .	24
Shock Wave Development . . . . .	24
Two-Dimensional Rectangular . . . . .	25
One-Dimensional Cylindrical . . . . .	32
One-Dimensional Spherical . . . . .	34
Geometry Used . . . . .	35
Computational Mesh Characteristics . . . . .	38
Dimensions . . . . .	38
Resolution . . . . .	39
Boundary Conditions . . . . .	41

Calibration of Code . . . . .	41
Overpressure Calibration . . . . .	42
Impulse Calibration . . . . .	43
Interaction With Structures . . . . .	43
Modeling the Buildings . . . . .	44
Shock Reflections . . . . .	47
IV. Results . . . . .	54
CTH Code Performance . . . . .	54
Reflected Overpressures . . . . .	55
Impulse . . . . .	59
V. Conclusions and Recommendations . . . . .	64
Conclusions . . . . .	64
Recommendations . . . . .	67
Appendix A: Sample CTH Files . . . . .	70
Appendix B: Tips on Using CTH . . . . .	84
Appendix C: Calibration of Code . . . . .	88
Bibliography . . . . .	92
Vita . . . . .	94

## *List of Figures*

	Page
Figure 1. L-Shaped Building . . . . .	5
Figure 2. Building With Separated Wings . . . . .	6
Figure 3. Example of Atrium Building in Two-Dimensional Rectangular Mesh . .	8
Figure 4. Major CTH Code Modules . . . . .	11
Figure 5. Remap of Distorted Mesh . . . . .	15
Figure 6. Ideal Blast Wave (5:84) . . . . .	18
Figure 7. Regular Reflection of a Plane Shock from a Rigid Wall (2:11) . . . .	19
Figure 8. Mach Stem Growth (5:89) . . . . .	21
Figure 9. Contact Surface Burst Blast Wave (5:92) . . . . .	21
Figure 10. Shock Developed Using Block of 2 Atmospheres Pressure Air 10 Meters Wide . . . . .	27
Figure 11. Density versus Distance for a Shock Wave . . . . .	28
Figure 12. Overpressure versus Range, Two-Dimensional Rectangular Shocks .	33
Figure 13. Overpressure versus Range, One-Dimensional Cylindrical and Spherical Shocks . . . . .	34
Figure 14. High Overpressure (1.02 Atmosphere) Shock . . . . .	37
Figure 15. Low Overpressure (0.46 Atmosphere) Shock . . . . .	37
Figure 16. Impulse (X Component) versus Y Dimension Width . . . . .	40
Figure 17. Long Rectangular Building Used for Code Calibration . . . . .	42
Figure 18. Additional L-Shape Buildings . . . . .	45

Figure 19. Legend for Pressure Contour Plots . . . . .	48
Figure 20. Shock Striking Atrium Building, Frame 1 . . . . .	49
Figure 21. Shock Striking Atrium Building, Frame 2 . . . . .	50
Figure 22. Shock Striking Atrium Building, Frame 3 . . . . .	51
Figure 23. Shock Striking Atrium Building, Frame 4 . . . . .	52
Figure 24. Reflected Overpressure versus Rotation Angle, L-Shaped Building .	57
Figure 25. Peak Overpressure on Walls of Atrium Building . . . . .	58
Figure 26. Impulse versus Rotation Angle, L-Shaped Building . . . . .	60
Figure 27. Impulse versus Separation Distance, Atrium Building . . . . .	62
Figure 28. Shimmed Wall Design . . . . .	68

## *List of Tables*

Table	Page
1. Shock Parameters: CTH Values Compared to One Kiloton Reference .....	31
2. Overpressure versus Range for Shock Waves Developed .....	32
3. Reflected Overpressures, L-Shaped Building .....	56
4. Peak Overpressure on Walls, Atrium Building .....	58
5. Impulse, L-Shaped Building .....	60
6. Impulse, Atrium Building .....	62



*Abstract*

This study investigated the interaction of shock waves with L-shaped structures using the CTH hydrodynamics code developed by Sandia National Laboratories. Shock waves traveling through air were developed using techniques similar to shock tube experiments. Models of L-shaped buildings were used to determine overpressures achieved by the reflecting shock versus angle of incidence of the shock front at five specific angles, ranging from zero to ninety degrees.

Calibration models were developed to determine the effects of mesh resolution and flow restriction on results. Models of rectangular box-shaped buildings were used to compare the overpressure and impulse computed by CTH to compilations of experimental and theoretical data contained in Wilfred E. Baker's *Explosions in Air*.

An L-shaped building model rotated 45 degrees to the planar shock front produced the highest reflected overpressure of 9.73 atmospheres in the corner joining the two wings, a value 9.5 times the incident overpressure of 1.02 atmospheres. The same L-shaped building was modeled with the two wings separated by 4.24 meters to simulate an atrium. This open courtyard provided a relief path for the incident shock wave, creating a peak overpressure of only 4.86 atmospheres on the building's wall surfaces from the same 1.02 atmosphere overpressure incident shock.

# SHOCK WAVE INTERACTION WITH L-SHAPED STRUCTURES

## I. *Introduction*

### *Background*

The overpressure of a shock wave amplifies when the shock wave strikes a rigid boundary. This amplification can severely damage structures at large distances from an explosion. Damage to structures occurs from two related forces: the diffraction loading and the dynamic pressure loading. Diffraction loading comes from the pressure difference between the front and rear faces of a structure as the shock wave envelops it. Dynamic pressure loading, also known as drag loading, is caused by the high wind speeds behind the shock front. One or the other of these two forces usually dominates depending on the size and shape of a structure. The drag forces due to the shape of a structure can be very large for long thin objects such as telephone poles or bridge girders, but diffraction loading is much larger than drag loading for large, enclosed buildings.

To date, experimental efforts have concentrated on determining the magnitude of the overpressure reflecting from a single flat surface at an angle of incidence between zero and ninety degrees. Extrapolation of this experimental data to more complex structures involving two or more walls and concave corners is difficult because reflections can combine into a mach stem, which changes the pressure pattern.

Although the hydrodynamics equations governing shock waves are well known, simulations of shock wave - building interactions are computationally expensive. Early codes could handle only very simple one-dimensional problems. Current codes can handle two- and three-dimensional problems, but the large number of calculations involved in transporting a shock wave a short distance quickly overload most workstations and minicomputers.

The Defense Nuclear Agency (DNA/SPWE) is sponsoring a three year AFIT project, one goal of which is to evaluate existing hydrodynamics codes with two objectives in mind: determining the full capabilities of the existing codes, and using the codes to model complex structures to enhance the database available to weapons effects planners.

### *Problem and Scope*

The CTH code was developed by Sandia National Laboratories to model strong shock physics problems involving multiple materials and large material deformations in one, two and three dimensions. CTH has been used extensively for armor penetration tests and modeling of high-explosive driven fragments from munitions, but very little work has been done in modeling air blast effects from large detonations, either nuclear or conventional. Before DNA can place a production code in everyday use, extensive characterization must take place to determine it's capabilities and limitations.

The primary emphasis of this investigation was to use CTH to investigate the interaction of shock waves with L-shaped buildings. A general characterization of CTH's performance was characterized to determine the effects of varying mesh resolution, boundary conditions, and flow restrictions on the results of a model. Methods for obtaining the desired results such as air flow velocity patterns and time histories of the forces on a building model were developed. Shock waves that represented the blast wave from a one kiloton yield free air burst were developed in one -dimensional rectangular (1DR), cylindrical (1DC), and spherical (1DS) coordinate systems. Two shock waves, one with an overpressure of 1.02 atmospheres and one with an overpressure of 0.46 atmospheres, were modeled in two-dimensional rectangular (2DR) geometry.

Rectangular building shapes were used to compare the CTH results to literature values. The two shocks modeled in two-dimensional rectangular geometry were then run into the L-shaped structures and results analyzed. Results of interest included peak overpressure and impulse on an L-shaped building at various rotation angles, and the reduction in loading experienced by the same building with varying width atriums built between the building's wings to allow a relief path.

### *Approach*

The first step in determining CTH's capabilities was to accurately simulate the shock wave formed by a nuclear explosion. Once fully developed, the shock wave should have overpressures, overpressure positive phase duration, underpressure,

negative phase duration, dynamic pressure, and a dynamic pressure positive phase duration that can be compared to the shock wave characteristics of the one kiloton (kt) reference shock wave.

Computer models of L-shaped buildings were prepared in two-dimensional rectangular geometry, with the buildings modeled as infinitely tall structures. The buildings' widths and lengths were chosen to represent typical small buildings. No windows or hallways were included due to limitations of the computational mesh size, so the buildings were modeled as solid blocks combined into the desired shapes.

The performance of CTH was characterized with respect to the geometry of the problem, boundary conditions, mesh size, and the flow restrictions caused by the building impeding the shock flow. Results were compared to literature values to determine appropriate use of the many modeling options available within CTH. Efforts to optimize the above parameters to decrease run time allowed use of finer mesh resolution without significantly increasing computation time.

Of equal importance, operational procedures were developed to work within the resource constraints of the SUN computer network, particularly the limited disk space. Electronic file transfer and large (3.2 gigabyte) archive tapes were used to preserve data. Backup restart files were used to recover and complete models that had crashed due to disk overflow.

After proof testing of the code, two investigations of shock interactions with L-shaped structures were accomplished. In the first phase, an L-shaped building with wings of 20 meters and 30 meters in length was modeled (See Figure 1).

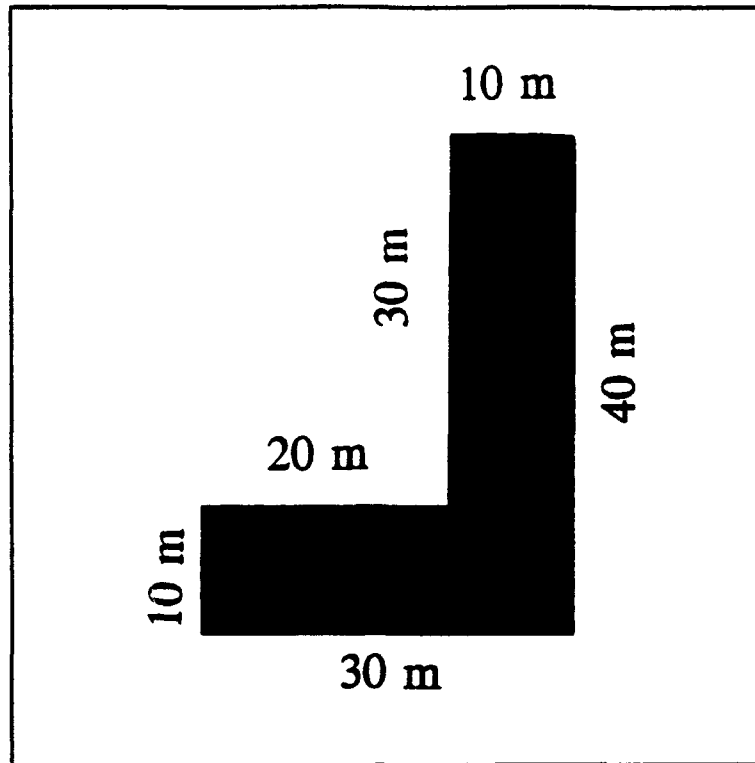


**Figure 1. L-Shaped Building**

A width for the two wings of 10 meters was chosen as representative of typical construction. The corner angle was held fixed at 90 degrees, and the building was then rotated from 0 degrees through angles of 22.5, 45, 67.5 and 90 degrees before being exposed to the advancing shock wave. Shock overpressures, flow patterns, and the forces on the building were investigated. In the second phase, the corner of the building was removed to simulate an atrium connecting the two wings (See Figure 2).

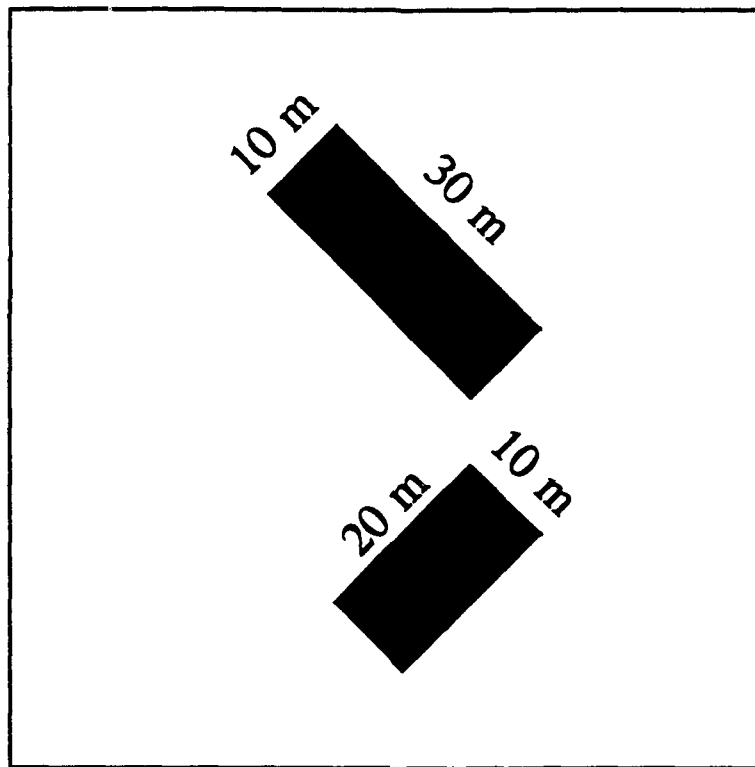


**Figure 2. Building With Separated Wings**

The open space between the wings provides a relief passage for the overpressure and dynamic pressure, which should lessen the impulse delivered to the wings of the building. Several different atrium widths were modeled to determine whether increasing the width of the gap would decrease the overpressure and impulse. Peak overpressure and impulse for the atrium building was determined for the building rotated at a 45 degree angle, since this angle resulted in the highest overpressure and impulse for the L-shaped building.

One building set at a specific rotation angle or atrium width and one of the two shock waves were combined in a two-dimensional rectangular computational

mesh for each shock - building interaction model, using a CTH code module called CTHREZ (See page 10 for further discussion of CTHREZ). Several characteristics of the two-dimensional rectangular mesh were common to all the L-shaped and atrium models: The Y dimension width was fixed at 150 meters, with the building's concave corner placed halfway between the Y boundaries at  $Y = 75$  meters. Because the overall X direction dimensions varied for the two shock waves, the  $X = 0$  plane was chosen to be where the building's concave corner was placed, with the shock front approaching from the left (negative X direction) and the shock wave out flowing past the building to the right in the positive X direction. Figure 3 shows a closeup view (full X and Y dimensions not shown) of an atrium building, in the two-dimensional rectangular mesh, being approached by the planar shock front. The two wings of the building are separated by 4.24 meters, each wing 2.12 meters from the  $Y = 75$  meters centerline. The two corners closest to the Y centerline are located on the  $X = 0$  plane, where the concave corner was located when the wings were joined. I refer to the area bounded by  $X = -50$  meters to  $X = 0$  and  $Y = 0$  to  $Y = 150$  meters as the impact zone, as this was the part of the mesh where the shock reflections of interest.



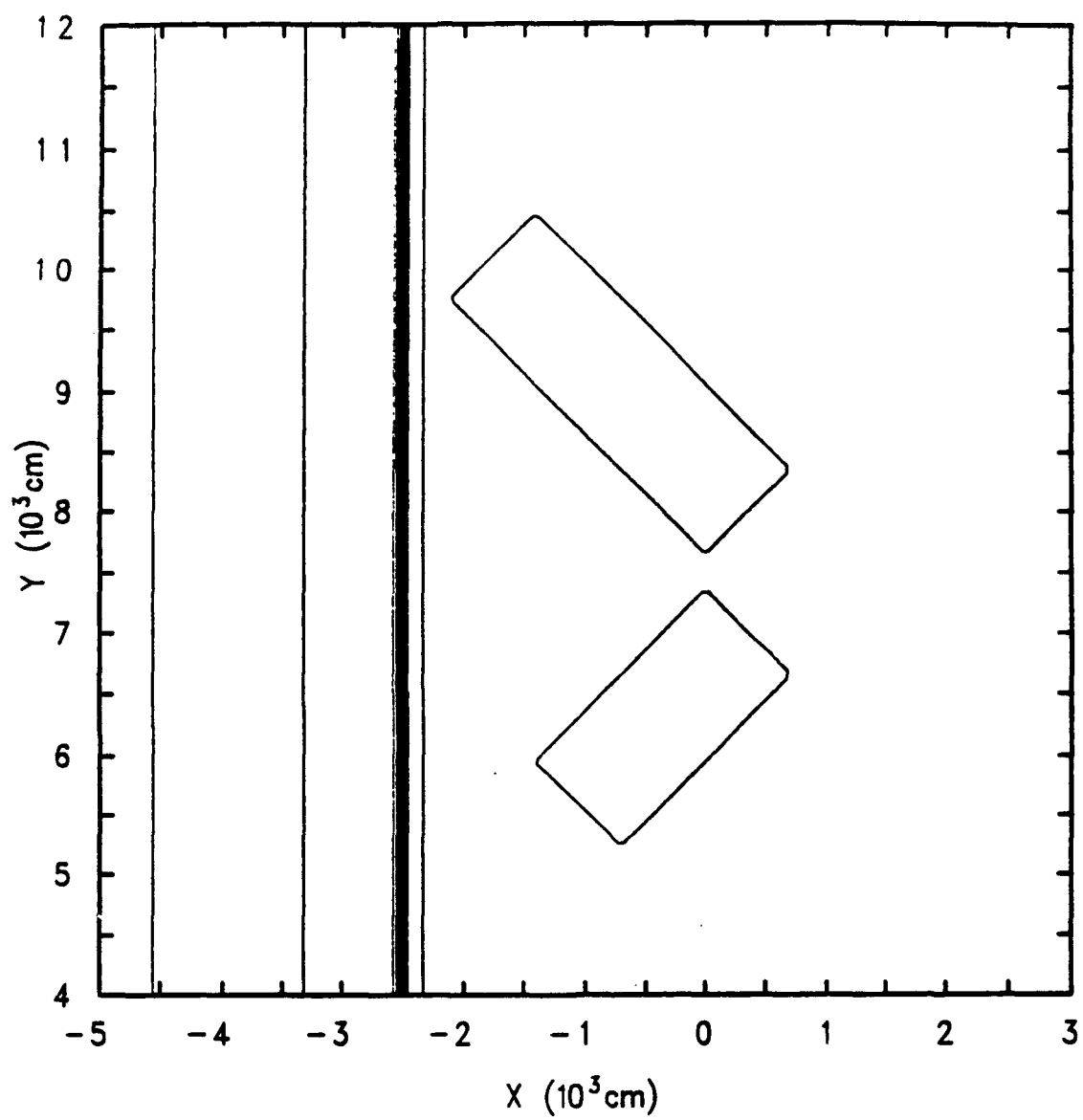


**Figure 3.** Example of Atrium Building in Two-Dimensional Rectangular Mesh

## II. *Theory*

A shock wave is created when the rapid release of energy by a chemical reaction, nuclear reaction, or mechanical process results in a pressure wave of finite amplitude. When the shock wave is traveling through air, the shock wave is commonly referred to as a blast wave (5:1). As the pressure disturbance travels through the surrounding air, the fact that air is a compressible gas causes the front of the pressure wave to steepen until it exhibits nearly discontinuous increases in pressure, density, and temperature (2:3). Additionally, the shock front travels faster than the speed of sound in the air, and accelerates the air particles in the direction the shock front is moving, creating a wind. Predicting the interactions of shock waves with structures involves three areas: the computational scheme used by CTH, ideal blast wave characteristics, and how shock waves reflect from objects and interact with other shock waves.

### *CTH's Computational Process*

There are two major parts to the CTH computational process. First, the outer loop consists of the key code modules used to generate, execute, rezone, and generate graphical output. The second loop is the inner loop, which consists of the three stage iterative loop used to perform the calculations which model the propagation of the shock wave through the air.

*CTH Code Modules.* There are six primary code modules used in developing a shock - building interaction model to be run in CTH (See Figure 4). The first module used is CTHGEN, which is used to generate the computational mesh, choose the thermodynamic model to be used, insert material such as the compressed air to create the shock wave and the material for the building, and specify all the other myriad details to be used for the model. The output file from CTHGEN is called a restart file that contains all the information required to run the model, whose default name is rscth.

This restart file is then used by the actual computational module, CTH, to run the model. Two key files are output by the CTH module: the extended rscth file, which now contains updated information concerning the state of the model, and the history file (default name hcth), which contains time histories of the state variables such as pressure, temperature, and density for the different materials in the model.

At this time, changes in the geometry, mesh size, or materials involved in the model can be made by using the rezone module, CTHREZ. Rezoning allows you to run a model for a certain number of time steps, change the parameters of the problem, then continue on with the model. This module supports some geometry changes, such as rezoning from one-dimensional cylindrical to two-dimensional rectangular, and also allows for insertion or deletion of materials. In this investigation, CTHREZ was commonly used to place the building in front of the fully formed shock wave, enabling reuse of the shock wave's restart file without having to

regenerate the shock wave each time. The output from CTHREZ is a modified restart file that can then be sent to the CTH module for further running of the model.

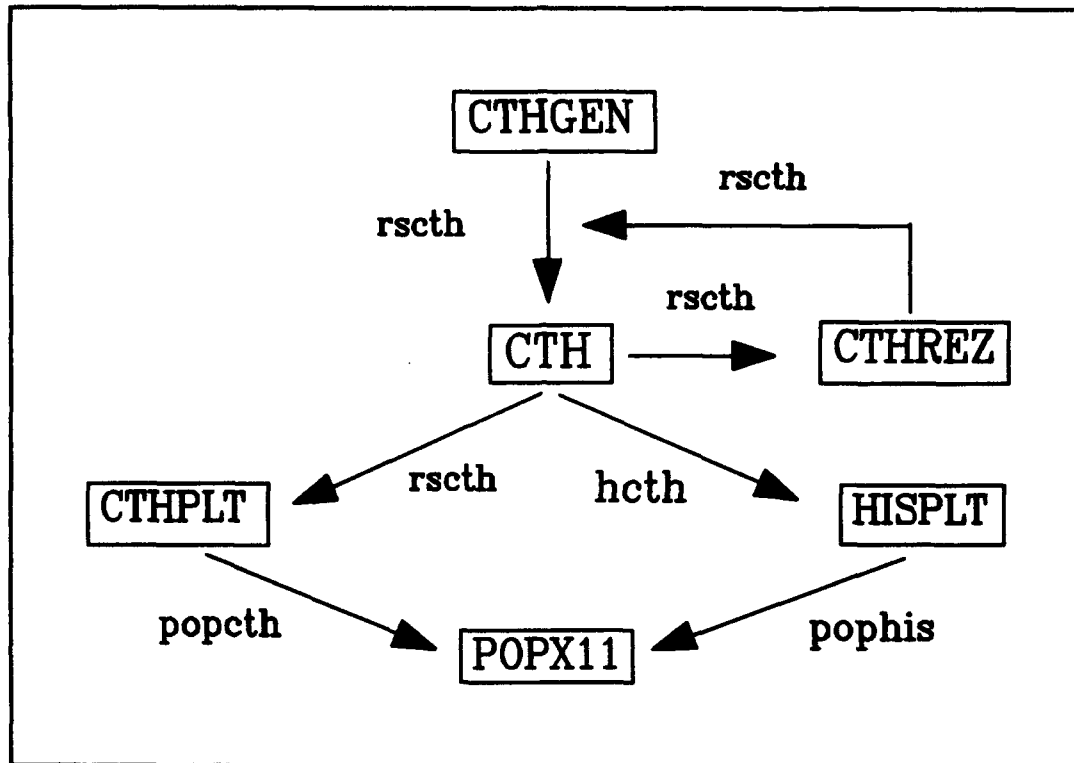


Figure 4. Major CTH Code Modules

Finally, data from the completed model can be analyzed using the three graphics modules. The module CTHPLT is used to process the restart file, and produces graphics such as pressure contour plots, which are placed in a file named popcth. The module HISPLT is used to create time history plots of the state variables from the history file, with the resulting plots placed in a file named pophis. These

two types of graphics files can then be viewed using a POP utility, such as POPX11 for the Sun workstations.

*CTH's Iterative Three Stage Computational Loop.* The motion of a shock wave through a hydrodynamic material can be modeled by solving a set of equations which relate the conservation of mass, momentum, energy, and volume. The CTH code models propagation of a shock wave in an iterative process in which each time step has three stages.

In the first stage, the Lagrangian forms of the conservation equations are solved, using finite volume approximations. First, the conservation of mass is expressed as

$$\frac{d}{dt} \int_{\beta} \rho dV = 0, \quad (1)$$

where  $t$  is the time,  $\rho$  is the mass density, and  $\beta$  is the configuration the Lagrangian body occupies at time  $t$ . (Note: The developers of CTH used the notation  $\beta_t$  to represent the configuration of the Lagrangian body at time  $t$ , but I have used  $\beta$  by itself for clarity of reproduction. Additionally, I will use the notation sometimes used in electrodynamics to differentiate between vectors and tensors. Vectors will have a single arrow over the variable, while tensors will have both a single arrow and be enclosed in braces.) Second, the conservation of momentum is represented by

$$\frac{d}{dt} \int_{\beta} \rho \vec{U} dV = \int_{\partial\beta} \hat{n} \cdot \{\vec{\Sigma}\} dA + \int_{\beta} \rho \vec{B} dV, \quad (2)$$

where  $\vec{U}$  is the velocity vector,  $\hat{n}$  is the unit normal vector,  $\{\vec{\Sigma}\}$  is the stress tensor,  $\partial\beta$  is the boundary of  $\beta$ , and  $\vec{B}$  is the body force vector. Third, the conservation of energy is represented by

$$\frac{d}{dt} \int_{\beta} \rho E dV = \int_{\beta} (\{\vec{\Sigma}\} \cdot \vec{\nabla}) \cdot \vec{U} dV + \int_{\beta} S dV, \quad (3)$$

where  $S$  is the energy source. Finally, CTH uses a fourth conservation equation: the conservation of volume is represented by

$$\frac{d}{dt} \int_{\beta} dV = \oint_{\partial\beta} \hat{n} \cdot \vec{U} dA, \quad (4)$$

where the rate of change of the volume equals the surface integral of the velocity normal to the surface of the Lagrangian body (10:13).

Two assumptions are used to further simplify the numerical solution of the above conservation equations. First, the material through which the shock propagates is assumed to be hydrodynamic. This allows the stress tensor,  $\{\vec{\Sigma}\}$ , to be replaced by the pressure,  $P$ , multiplied by the identity tensor,  $\{\vec{I}\}$ . The second assumption adds an artificial viscosity term to the conservation equations to help model irreversible processes associated with shock waves (10:15). The artificial viscosity is used as a dissipative mechanism to spread the nearly discontinuous jumps in pressure and density at the shock front over several computational cells. This helps the finite

difference solution model shock wave propagation with acceptable numerical stability.

The artificial viscosity is introduced using the equation

$$\{\bar{\Sigma}\} = -P\{\bar{I}\} - \{\bar{Q}\}, \quad (5)$$

where  $P$  is the pressure,  $\{\bar{I}\}$  is the identity tensor, and  $\{\bar{Q}\}$  is the artificial viscosity tensor. Substituting this relationship into the conservation equations changes equation (2) into

$$\frac{d}{dt} \int_{\beta} \rho \bar{U} dV = - \int_{\partial\beta} \hat{n} \cdot (P\{\bar{I}\} + \{\bar{Q}\}) dA + \int_{\beta} \bar{B} \rho dV, \quad (6)$$

and equation (3) becomes

$$\frac{d}{dt} \int_{\beta} \rho E dV = - \int_{\beta} P \bar{\nabla} \cdot \bar{U} dV - \int_{\beta} (\{\bar{Q}\} \cdot \bar{\nabla}) \cdot \bar{U} dV + \int_{\beta} S dV. \quad (7)$$

In this Lagrangian stage the mesh distorts and flows with the material based on the numerical solution to the conservation equations for all of the cells in the computational mesh.

In the second stage, the distorted cells are remapped back into the original mesh shape. The material masses, energies, and volumes are passed from the Lagrangian step to the remap step, then the thermodynamic properties of the new contents of the original mesh are computed using the equation of state and the thermodynamic model being used. Figure 5 shows first the original mesh, with a block of material spanning one and a half cells. In the center image, the block has

moved to the right and the mesh has distorted. Finally, in the right most image the mesh is remapped back to the original mesh, but the block of material remains in its new location.

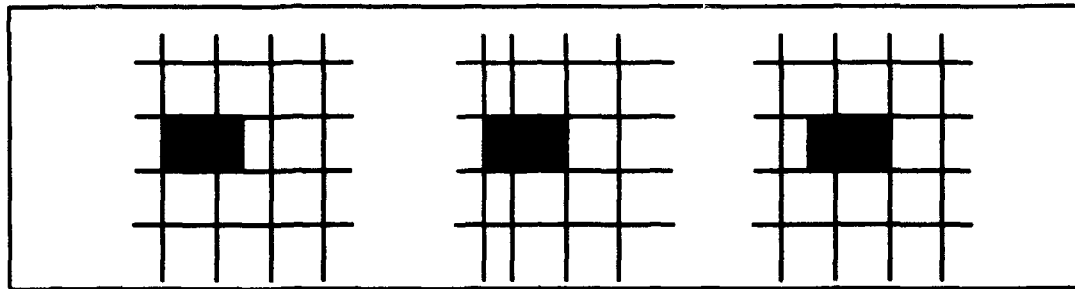


**Figure 5. Remap of Distorted Mesh**

Two equation of state models were used in this investigation: a tabular equation of state model called SESAME was used to approximate the thermodynamic properties of the air, and CTH's approximation to the Mie-Grüneisen equation of state was used to model the thermodynamic properties of the building material. The SESAME equation of state model provides a look-up table approach to modeling the complex high and low temperature properties of a material instead of attempting to use an equation to match temperature extremes and changes in state such as ionization. CTH's approximation of the Mie-Grüneisen equation of state was used to model the building material to permit changing material properties to create unnatural building materials, as discussed on page 45. CTH approximates the Mie-Grüneisen equation of state as



$$P(\rho, E) = P_R(\rho) + \Gamma(\rho) \rho [E - E_R(\rho)], \quad (8)$$

where  $P_R(\rho)$  and  $E_R(\rho)$  are the pressure and internal energy obtained from a reference curve and the Grüneisen parameter,  $\Gamma$ , is assumed to depend only on density. The dependence of the internal energy on temperature is defined by

$$E(\rho, T) = E_R(\rho) + C_V [T - T_R(\rho)], \quad (9)$$

where  $T_R(\rho)$  is the temperature along the reference curve, and the specific heat,  $C_V$ , is assumed constant (8:11).

Of the four thermodynamic models offered by CTH, the multiple material pressure (MMP) model was chosen for this investigation. The MMP model allows the different materials in a cell to have independent temperatures and pressures. There are no interactions between the different materials in a cell, and the volume change of a material calculated in the remap step is proportional to the material's volume fraction in a cell. The actual thermodynamic calculations for each material in a multi-material cell are then accomplished as if each material was a single unmixed cell (9:49). The other thermodynamic models available are the single material cell, the multiple material temperature model (MMT), and the single pressure and temperature (1PT) model. The single material cell model was inappropriate for this investigation because the slight building movements will place both air and the building material in cells at the interface. The 1PT and MMT models both use a complex iteration scheme that is computationally costly and frequently gives significant errors in problems with large temperature gradients and materials that vary

widely in compressibility. The MMP model has the advantage of being much faster to compute since only single material thermodynamics are used, and it frequently gives the most accurate answers because the thermodynamics are computed for each material separately. The biggest drawback to the MMP model is that two materials in a cell with different pressures will not equilibrate over time, as they should (9:51).

Finally, a third stage allows the user to modify the data base to change certain aspects of the problem, such as increasing an energy source or removing material below a certain density. CTH then returns to stage one and begins the cycle again.

### *Ideal Blast Wave*

Assuming an air blast is propagating through homogenous air and that the source is spherically symmetrical, the blast wave's characteristics will be functions only of the range,  $R$ , from the source and the time since the explosion,  $t$ . The ideal blast wave is commonly represented as a time history of the overpressure at some arbitrary distance from the explosion. Figure 6 shows the abrupt pressure rise at time  $t_s$ , the time the shock front arrives at that range from the explosion.

The pressure rises nearly instantaneously to the peak overpressure,  $p$ , then decays through the ambient pressure,  $P_0$  and decreases to a peak underpressure before returning to the ambient pressure (5:82). The ratio of the peak overpressure to the ambient pressure,  $p/P_0$ , is commonly used to describe the relative strength of a shock wave. When the ratio is large, a shock is described as strong. If the ratio is near one, the shock is described as weak (4:154). The time elapsed between the arrival

time and when the pressure falls through ambient is known as the positive phase duration,  $t_p^+$ , which will be represented as  $tp^+$  in equations for clarity in reproduction. The negative phase has a slightly longer duration than the positive phase.

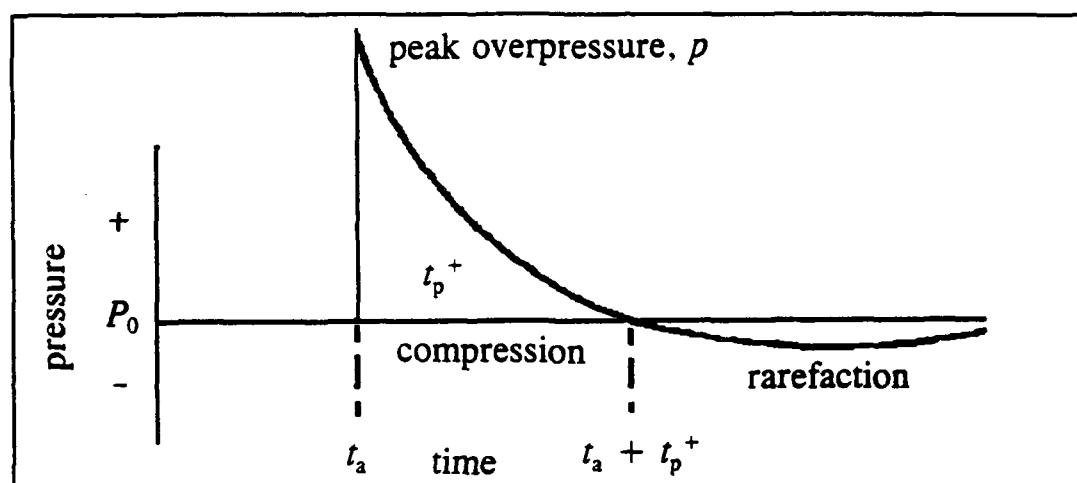


Figure 6. Ideal Blast Wave (5:84)

The impulse of a blast wave,  $I_p^+$ , depends on this time variation of the overpressure,  $p(t)$ , and is

$$I_p^+ = \int_0^{t_p^+} p(t) dt. \quad (10)$$

There is also a negative phase impulse, but it is usually neglected because most of the blast damage is caused by the much stronger impulse during the positive phase.

Typical damage from the underpressure (negative) phase involves weakly attached plaster or veneer coverings popping off of walls (5:86), whereas damage from the overpressure (positive) phase can involve total destruction of load-bearing walls.

### *Blast Wave Reflections*

When a blast wave strikes a flat surface head on (normal incidence) the peak value of the reflected overpressure is given by

$$p_r = 2p \cdot \frac{7P_0 + 4p}{7P_0 + p} \quad (11)$$

This indicates that at lower values of overpressure, the acoustic limit is observed and  $p_r = 2p$ . For blast waves with a higher overpressure ( $p \gg P_0$ ), the reflected overpressure approaches eight times the incident overpressure (5:99).

In still air, a blast wave striking a rigid wall obliquely with an angle of incidence,  $\alpha_i$ , not equal to  $0^\circ$  or  $90^\circ$  will reflect as shown in Figure 7. The pressure, density, and temperature of the air in region one will be that of the unshocked, ambient air. The air in region two has been shocked once, and finally, the air in region three has been shocked twice as the incident and reflected shocks move from left to right across the wall.

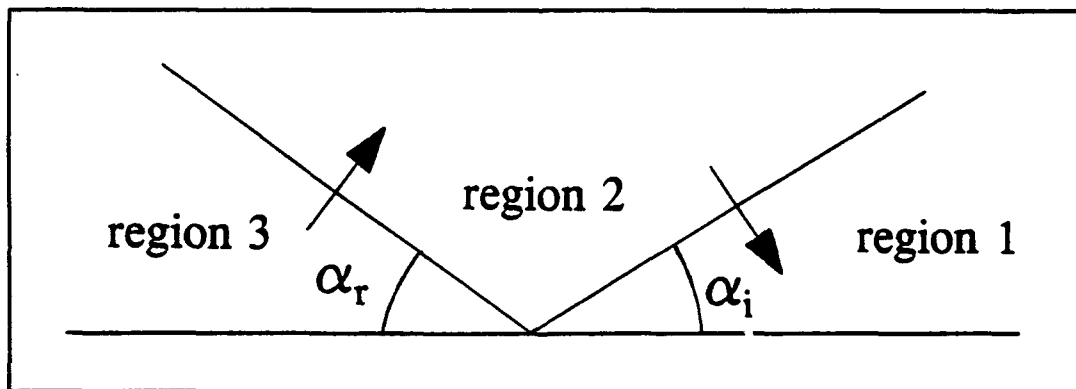


Figure 7. Regular Reflection of a Plane Shock from a Rigid Wall (2:11)

Two properties of a regularly reflected shock are important to the analysis of blast wave effects on structures. First, when the angle of incidence of a blast wave traveling through air exceeds  $39^{\circ} 23'$ , the peak overpressure of the reflected shock will be greater than for a normally incident ( $\alpha_i = 0^{\circ}$ ) shock (2:11). Second, when the angle of incidence is greater than a peak overpressure dependent critical angle (not necessarily equal to  $39^{\circ} 23'$ ), regular reflection cannot occur. Instead, a phenomenon known as Mach reflection occurs (2:11).

In Mach reflection, the reflected wave travels through shock heated air, in which the speed of sound is higher than the speed of sound for the ambient air. The speed of sound,  $a$ , in a perfect gas is dependent only on the temperature of the gas, as shown by

$$a = \sqrt{\gamma RT}, \quad (12)$$

where  $\gamma$  is the ratio of the specific heats for the gas,  $R$  is the universal gas constant, and  $T$  is the absolute temperature (1:89). This difference in the sound speed of the shocked and unshocked air allows the reflected blast wave to catch up to the incident blast wave and merge into what is known as the Mach stem. As the incident shock front travels away from the explosion, the Mach stem grows as shown in Figure 8. The point where the reflected shock, incident shock, and Mach stem all meet is called the triple point (5:89). For structures below the height of the triple point, only a single shock passage will be felt.

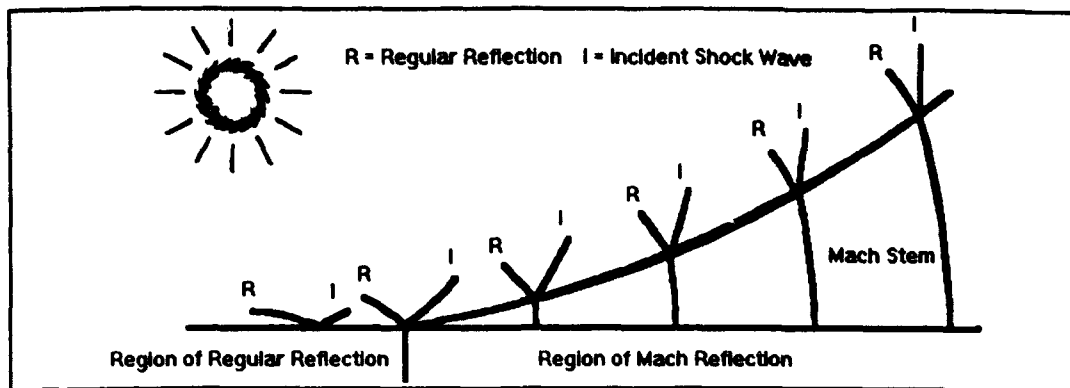


**Figure 8. Mach Stem Growth (5:89)**

A shock front similar to Mach reflection is created by a contact surface burst. When the explosion occurs at the surface, the incident and reflected waves coincide instantly and structures on the surface are subjected to an air blast similar to the Mach stem (See Figure 9). A blast wave from a contact surface burst, traveling over an ideal surface, will have shock front characteristics such as overpressure and dynamic pressure that correspond to a free air burst of twice the energy yield (5:91).

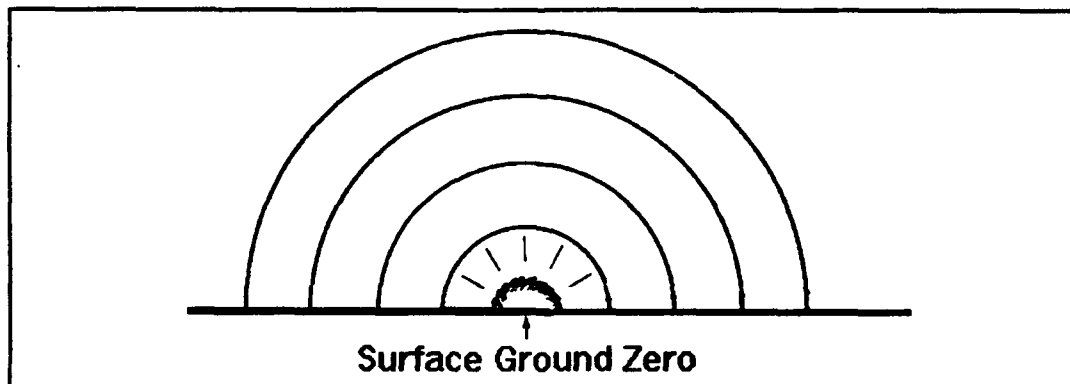


**Figure 9. Contact Surface Burst Blast Wave (5:92)**

### *Horizontal Loading of Structures*

There are two steps to determining the effect a strong shock wave will have on a structure. First, the loading caused by the airblast must be determined. This is dependent on the shape and size of the building, as well as the strength of the shock. Second, the structural response of the building must be determined.

The airblast loading is a function of the peak overpressure, the dynamic pressure, the rate of decay of the overpressure, and the duration of the overpressure. Although these characteristics are identical for a given shock wave, the blast loading a building experiences depends on the size, shape, orientation, and material response of the structure. Traditionally, the theory of airblast loading has been supported primarily by experimental data from shock tubes and wind tunnels (10:132). Two- and three-dimensional hydrodynamics codes enable examination of shock - building interactions in a more efficient manner.

There are two significant aspects to the horizontal loading on a building: diffraction loading due to the pressure differences between the front and rear faces of the building as the shock wave envelops the building, and drag loading due to the wind rushing past the structure. The diffraction loading is highest when the reflected pressure on the front face is at its peak and the pressure on the rear face is still ambient because the blast wave has not completely engulfed the building and reached the rear face. For a closed structure, the duration of the diffraction loading will be approximately the time it takes for the shock front to travel from the front face to the rear face of the building (5:130). The drag loading acts for a longer period of time,

throughout the positive phase of the shock and slightly into the negative phase.

However, because the dynamic pressure is usually much less than the overpressure, diffraction loading is the dominant force on large, closed buildings (5:135).

The structural response of a building to the blast wave is highly dependent on the methods and materials of construction. Combinations of materials and construction techniques in a single building would require very detailed modeling, well beyond the scope of this investigation. However, simplified modeling of the shape of the structure to determine the peak overpressures and loadings may enable a rough estimate as a starting point for more detailed analysis of the probability of damage to a complex structure based on the type of construction.



### III. *Investigation*

The CTH code has been widely used for strong shock physics modeling at Sandia National Laboratories, and is a very capable code for performing hydrodynamic calculations with its ability to model material strength, fracture, distended materials, and high explosives (3:Abstract). The primary question of this investigation was therefore not whether or not CTH was capable of performing analysis of blast wave interactions with complex structures, but rather how to model shock waves and buildings in CTH, and then to look at the effects of the shock waves striking the buildings. To accomplish this goal, three broad areas were investigated: shock wave development, development of a benchmark model that could be compared to compilations of experimental and theoretical data, and interaction of shock waves with L-shaped structures.

#### *Shock Wave Development*

The first step in the investigation was to determine how best to model the blast wave from a nuclear explosion. The one kiloton reference blast wave is a compilation of experimental, theoretical, and computed data which describes the characteristics of a free air burst of one kiloton yield. A yield of one kiloton was chosen as a reference case because it simplifies scaling of blast wave characteristics. The one kiloton reference blast wave is modeled in a three-dimensional spherical coordinate system as a symmetrically expanding spherical wave. As such, the blast

wave's characteristics are dependent only on the range of the shock front from the explosion's origin, as described for the ideal blast wave (See page 17). However, three-dimensional spherical geometry is not supported by CTH, so some compromise must be made in developing a model of the one kiloton reference blast wave. There were two concerns in whether a CTH supported geometry would be useful for modeling air shock - building interactions. First, complex shapes must be supported for insertion of buildings. The second consideration in choosing a geometry was the ability to model a realistic shock. Buildings can be modeled in three potential geometries supported by CTH: two-dimensional rectangular, two-dimensional cylindrical, and three-dimensional rectangular. Shock waves could be modeled in the one-dimensional counterparts to each of the above geometries.

*Two-Dimensional Rectangular.* CTH's two-dimensional rectangular coordinate system supports six shapes for material insertion: box, circle, ellipse, parallelogram, triangle, and a user defined shape. Combinations of these shapes allows construction of very complex structures. The user defined shape is a powerful tool for building modeling which allows the user to input up to 100 vertices. The vertices are then connected sequentially with straight lines, starting with the first point entered, and closing the figure by connecting the last point entered to the first point. Figure 1, the L-shaped building, is an example of a user defined shape with six vertices. Additionally, a rotation center can be chosen, and the entire figure rotated to any desired angle.

One-dimensional rectangular geometry was used to develop shock waves to save computational time. After the parameters to produce the desired shock wave in one-dimensional rectangular were determined, the shock was then modeled in two-dimensional rectangular geometry to be used for shock - building interactions. The shock front produced by this technique simulates a small solid angle section of a spherically expanding blast wave under three conditions: for a target at the same altitude as an air burst, for a ground target within the Mach stem of an air burst, or for the shock wave from a contact surface burst striking a ground target.

Two techniques were used to develop a model of an ideal blast wave in one-dimensional rectangular geometry. The first was to increase the pressure and temperature of the air in a block of cells at the origin, simulating the heat and pressure of a nuclear explosion, then releasing the box of air into a mesh filled with air at ambient temperature (298 K) and pressure (1 atmosphere). The density in both the compressed region and the ambient region were set equal. This technique developed a shock front that looked appropriate, but did not create a negative phase and return to ambient pressure like the ideal blast wave in Figure 6. Instead the pressure decayed slowly towards the ambient pressure (See Figure 10).

The second technique was one commonly used in shock tube experiments. The pressure was increased in the compressed air section, and this time the temperature was set equal to the temperature in the ambient section while the air density in the compressed section was increased proportional to the pressure increase.

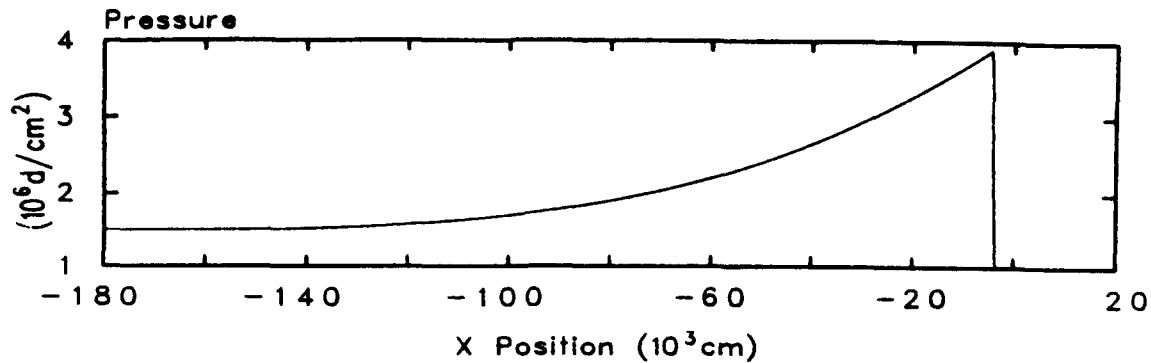


**Figure 10.** Shock Developed Using Block of 2 Atmospheres Pressure Air 10 Meters Wide

For example, an increase of pressure to six times ambient was matched with an increase in density to six times ambient to keep the temperature in both sections equal. This technique resulted in a shock with overpressure characteristics much closer to the ideal blast wave. A definite negative phase was present, and the magnitude of the underpressure was within the 0.27 atmospheres guideline suggested by Glasstone (5:82). However, the large difference in densities between the two sections produced a contact surface discontinuity between the compressed region and the ambient region, just as occurs in a shock tube experiment. A contact surface separates two regions of gas with no gas flowing across the contact surface. A shock front has the same type of discontinuous jump in density, but gas does flow across the shock front (4:119). Fortunately, effects of the density contact discontinuity (shown in Figure 11 at  $X = -17500$  cm) were easily removed from the model using one of two methods, depending on the other model parameters.

For the lower pressure shock, the contact surface was removed from the problem when the mesh was rezoned and the building inserted. Once gone, there was no way for it to influence the model. For the higher pressure shock, removing the contact surface by rezoning caused densities below the limits of the air SESAME table. However, because the contact surface moves much slower than the shock front, the problem stop time was reached before the contact surface moved more than a few meters from its original position. This small movement prevented the unwanted density discontinuity from getting close to the area of interest near the building, where it might have affected the shock - building interactions.

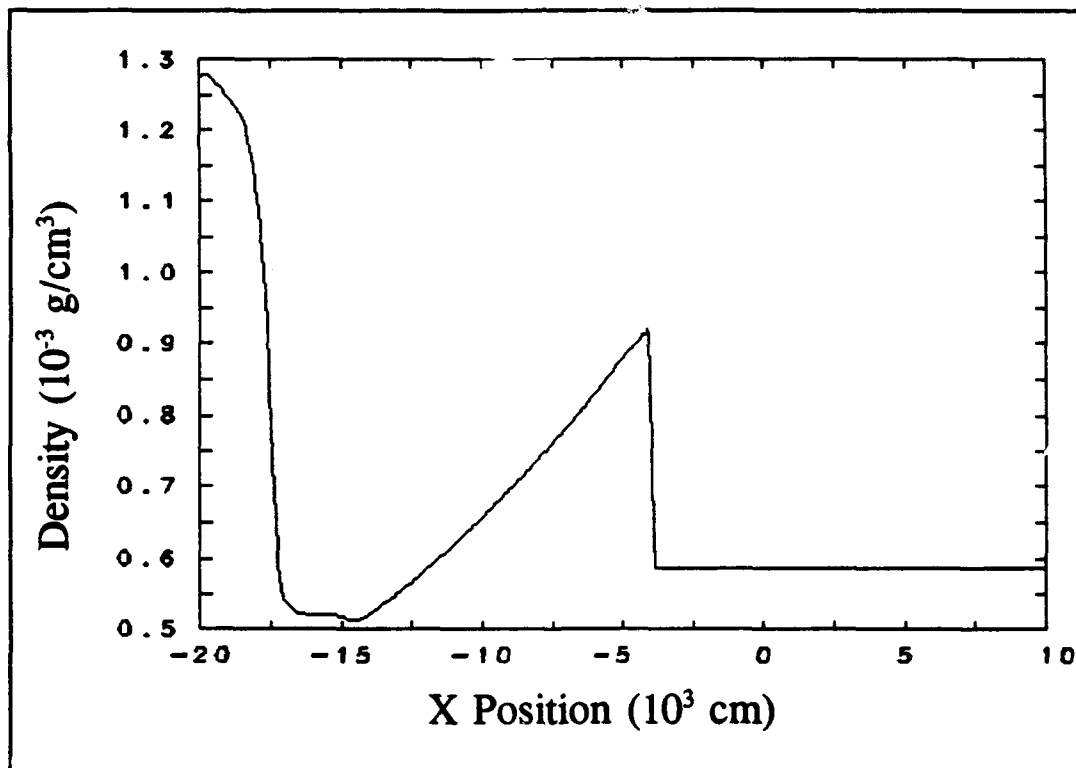


Figure 11. Density versus Distance for a Shock Wave

Adjustment of the shock characteristics was possible by selecting different combinations of pressure and width for the compressed section. This allowed setting the values of the shock parameters (overpressure and positive phase duration) at the point in the mesh where the shock front impacts the building. A general algorithm for building additional shock waves using this method starts with setting up a one-dimensional rectangular geometry mesh of 1000 cells with  $X$  varying from zero to 1000 meters. Tracers are then placed every 100 meters through the mesh. A compressed air region is created in the 10 cells from  $X=0$  to  $X=10$  meters, with the pressure equal to six times the desired overpressure at the impact zone. The density in the compressed region is also set at six times the ambient density. For example, if a one atmosphere overpressure is desired at the impact point of the mesh, air with a pressure of six atmospheres and a density six times the ambient density would be inserted into the mesh as a 10 meter wide box. Ambient air is inserted into the remaining mesh. After the problem is run, the pressure histories at the tracers are examined to look for a fully developed shock wave. The tracer that has the overpressure and positive phase duration closest to the desired characteristics is chosen as the impact point. The overpressure at that point is then adjusted by changing the pressure and density values in the compressed region, typically keeping both pressure and density the same multiple times ambient, and running the problem again. Once the overpressure at the impact zone is close to the desired value, the positive phase duration can be adjusted by changing the width of the compressed region, while keeping the pressure and density fixed at the value chosen in the step

above. Increasing the width typically increases the positive phase duration of the shock wave. Decreasing the width tends to decrease the positive phase duration. However, large changes in the width of the compressed region will change the value of the overpressure at the impact point, so some fine tuning of pressure, density, and compressed region width may be required. For example, a compressed air region 8 meters wide with a pressure and density 6.3 times ambient produced a shock wave with an overpressure of 1.02 atmospheres and a positive phase duration of 0.174 seconds.

For this investigation, values of overpressure and corresponding positive phase duration were selected to match the one kiloton free air blast wave to facilitate comparison to experimental data. Some shock characteristics could not be controlled and did not match well: the shock velocity,  $U$ , and the dynamic phase duration,  $t_q^+$ . The shock velocity is the velocity of the shock front as it travels away from the burst location. Because the shock is traveling faster than predicted by the one kiloton reference standard, the shock envelops the building more quickly than it should. This could affect the horizontal loading on the building, since the rear face of the building begins to feel a pressure increase more quickly than predicted. The dynamic phase duration is the period of time in which the wind behind the shock front is blowing in the same direction as the shock is moving, and therefore is the time period during which drag loading of the building occurs. Table 1 shows a comparison between the shock parameters computed by CTH for the two shocks used in the investigation and the shock parameters for the one kiloton reference blast wave at the corresponding

ranges from the detonation. The values for the one kiloton reference blast wave were read from Figures 3.55 and 3.72 in *The Effects of Nuclear Weapons* (5:98,109), except for the positive and dynamic phase durations, which were obtained through discussions with Dr. Charles J. Bridgman.

Table 1

Shock Parameters: CTH Values Compared to One Kiloton Reference Blast Wave				
Shock Parameter	1.02 Atmosphere Overpressure Shock: Range = 210 meters		0.46 Atmosphere Overpressure Shock: Range = 300 meters	
	CTH Value	1 kt Reference	CTH Value	1 kt Reference
overpressure (atm)	1.02	1.02	0.46	0.47
$t_p^+$ (sec)	0.174	0.179	0.212	0.22
$t_q^+$ (sec)	0.18	0.28	0.22	0.30
$U$ (m/sec)	685	460	625	400

Because the diffraction loading is much larger than the drag loading for the types of buildings modeled, the short dynamic phase should not significantly affect the results. In addition to these characteristics not matching the one kiloton reference blast wave, the peak overpressure of the two-dimensional rectangular shock wave did not decrease as rapidly as the reference blast wave. I believe this effect and the higher than expected shock speed relate to the lack of spherical spreading of the shock that occurs in a three-dimensional spherical geometry. Figure 12 and Table 2 show the decrease



in overpressure with increasing distance from the burst for the two shocks used in my investigation. The comparison values for the one kiloton reference blast wave were read from Figure 3.72 in *The Effects of Nuclear Weapons* (5:109).

Table 2

Overpressure versus Range for Shock Waves Developed					
Range (m)	Geometry of Shock				
	1 kt Reference (atm)	1.02 Atm 2DR (atm)	0.46 Atm 2DR (atm)	1DC (atm)	1DS (atm)
100	5.78	1.35	0.70	1.80	3.70
200	1.22	1.02	0.68	0.74	0.88
300	0.54	0.8	0.58	0.48	0.48
400	0.34	0.7	0.46	0.35	0.30
500	0.24	0.65	0.44	0.28	0.22
600	0.17	0.56	0.38	0.23	0.17
700	0.14	0.53	0.36	0.20	0.14
800	0.12		0.35	0.18	0.12

*One-Dimensional Cylindrical.* Modeling a shock in one-dimensional cylindrical geometry provided more spreading with increased range. This produced a shock whose peak overpressure decreased more rapidly than the two-dimensional rectangular shocks, but still not as rapidly as the one kiloton reference blast wave as shown in Figure 13 and Table 2. A fairly realistic shock with a negative phase could

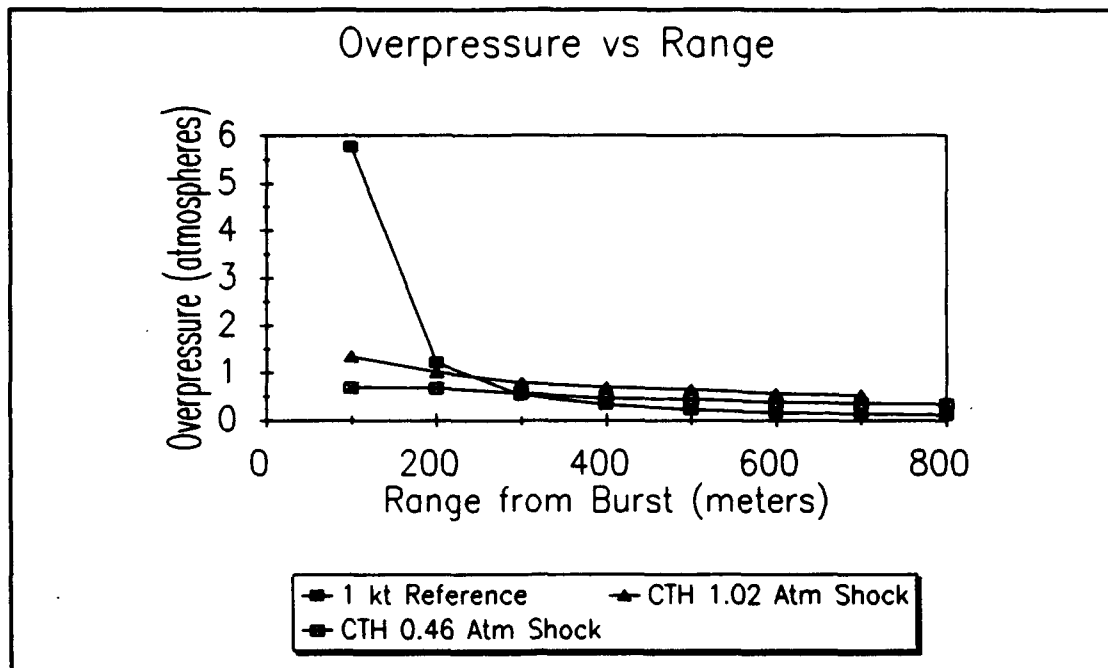


**Figure 12. Overpressure versus Range, Two-Dimensional Rectangular Shocks**

be produced merely by increasing the pressure and temperature of the compressed region, with 22 meters of air compressed to 16 atmospheres being used. The conversion from one-dimensional cylindrical to two-dimensional rectangular is supported by CTH, which allows for the insertion of a wide variety of building shapes. However, because the shock front is no longer planar when inserted into a two-dimensional rectangular mesh, reflections from the  $Y=0$  and  $Y=150$  meter walls quickly distorted the shock into an unusable form. Because the shock was unusable, no effort was made to match the other shock parameters to the one kiloton reference standard.

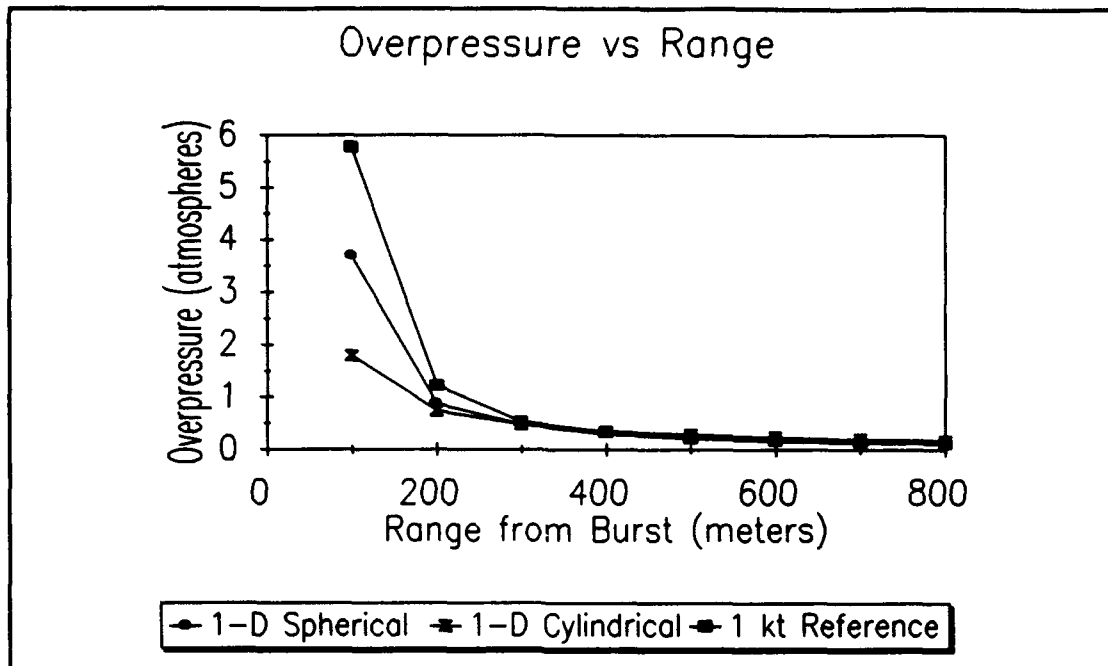


**Figure 13.** Overpressure versus Range, One-Dimensional Cylindrical and Spherical Shocks

*One-Dimensional Spherical.* Development of a shock wave in one-dimensional spherical geometry held the most promise for modeling the one kiloton reference blast wave. A shock wave whose overpressure decreased with range similar to the one kiloton reference blast wave (See Figure 13 and Table 2) was developed using 26 meters of air compressed to 75 atmospheres. However, although CTH was able to rezone the one-dimensional spherical shock wave into a three-dimensional rectangular mesh, the rezone module had a bug that would not allow insertion of the building, so no further development of this shock was accomplished. Unlike the technique used for two-dimensional rectangular geometry shock waves, it is much harder to control the positive phase duration in one-dimensional spherical geometry. This requires

many trials with varying parameters to match the one kiloton reference standard. Because of the rezone module problem, no further effort was expended trying to match the other parameters of the one kiloton reference blast wave. Some modeling in three-dimensional rectangular geometry was done where the shock and building were both generated at the same time to avoid the rezone module. Unfortunately, there was no way to translate the shock parameters used to create a shock in one-dimensional spherical geometry to three-dimensional rectangular geometry, so shock development required full three-dimensional calculations. Because the time required to run a three-dimensional model is extremely large (See page 55), only a few models were run with 10 and 20 cubic meter mesh cells, which were far too coarse to provide meaningful data. These models did show the possibility of creating a shock this way, but to do so would require tremendous computational costs.

*Geometry Used.* The need to model complex buildings limits the choice of geometry to two-dimensional or three-dimensional rectangular. Although the shocks developed in one-dimensional cylindrical and spherical geometries could be rezoned to two-dimensional and three-dimensional rectangular respectively, problems in shock propagation or high computing costs made these geometries poor choices. Therefore, two-dimensional rectangular geometry was chosen, even though it provides a peak overpressure and positive phase duration that match the one kiloton blast wave only at the building's corner. This was considered to be an acceptable limitation since the peak reflected overpressure was located either in the corner for the L-shaped building or within 3 meters for the atrium building.

Two shocks were developed in two-dimensional rectangular geometry and used for further analysis. The higher pressure (strong) shock has an overpressure of 1.02 atmospheres and a positive phase duration of 0.174 seconds at the impact point. The lower pressure (weak) shock has an overpressure of 0.46 atmospheres and a positive phase duration of 0.212 seconds. These characteristics were chosen to match those of the one kiloton reference air blast at a distance of 210 meters for the higher pressure shock and 300 meters for the lower pressure shock. The negative phase remains within 0.27 atmospheres of the ambient pressure for both shocks, but appears to be of shorter than normal duration. Pressure histories at the mesh's impact point ( $X = 0$  meters) are shown in Figure 14 and Figure 15. The x points on both graphs show the decay of the shock overpressure with time as predicted by Air Force Systems Command Manual 500-8 (12:3-6).

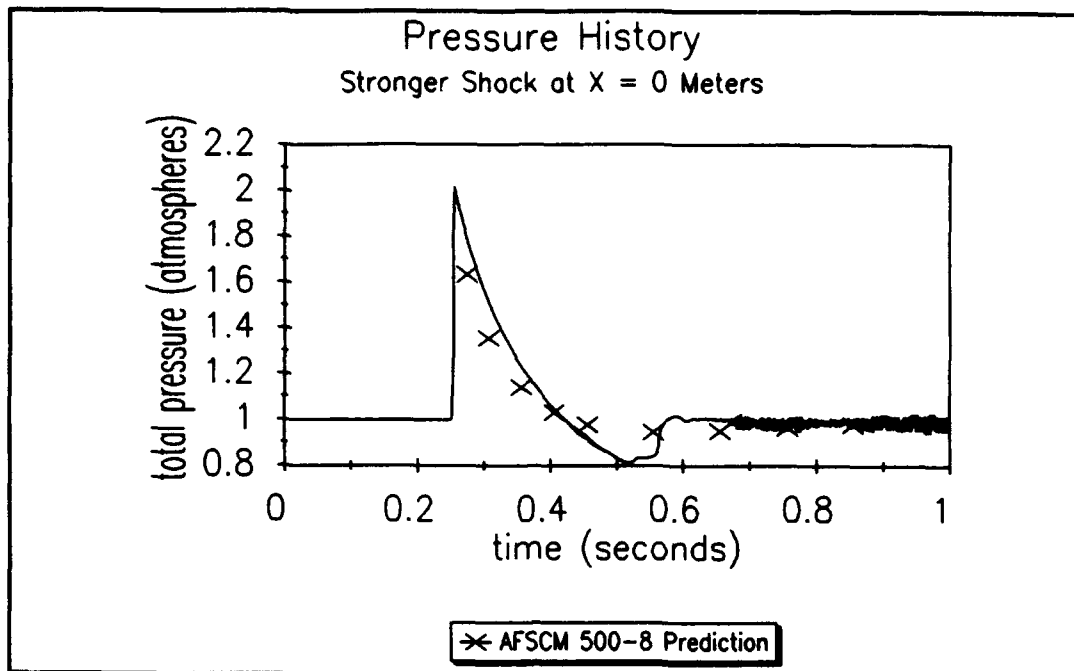


**Figure 14. High Overpressure (1.02 Atmosphere) Shock**

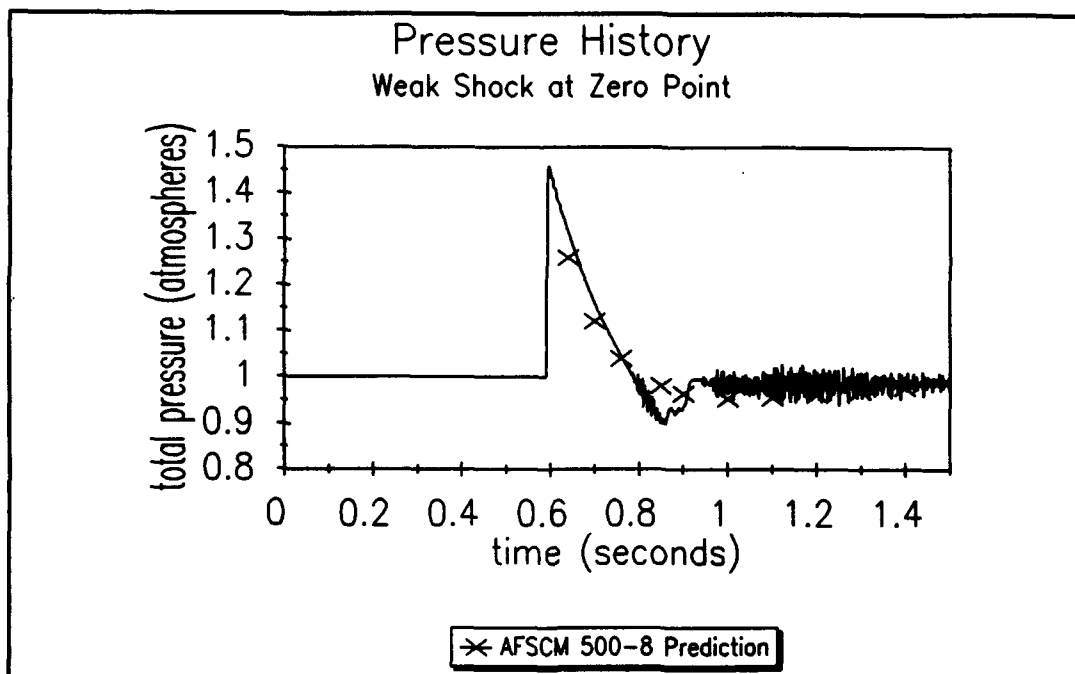


**Figure 15. Low Overpressure (0.46 Atmosphere) Shock**

Attempts at creating a shock with an overpressure above 1.5 atmospheres using various pressure, density, and temperature combinations for the compressed air led to limited success, in that the peak overpressure could be achieved, but the shock lacked a negative phase. Eventually the low air density region between the compressed air region and the negative phase of the shock wave (See Figure 11) exceeds the limits of the SESAME table used to model the air's thermodynamic properties. CTH then stops the computation because the equation of state model is outside the valid range, effectively limiting the strength of shocks that can be created using the techniques of this investigation.

#### *Computational Mesh Characteristics*

Once two-dimensional rectangular was chosen as the appropriate geometry to use for modeling the shock-building interactions, the mesh dimensions, mesh resolution, and appropriate boundary conditions were determined.

*Dimensions.* The appropriate X dimension width was determined primarily by the depth of the fully developed shock front. The stronger shock was approximately 125 meters deep from the face of the shock front to the end of the negative phase. The weaker shock was approximately 250 meters deep. Additional distances were added to allow the shock to propagate in the new mesh before striking the building, for the impact zone of the building, and finally to allow the air to flow around the building and resume its direction before flowing out of the mesh. The final X

dimension widths were 300 meters for the strong shock and 450 meters for the weaker shock.

The Y dimension width was determined solely by the need to eliminate errors due to flow restriction, where the building disturbs the shock wave's flow such that reflections from the boundaries cause errors in the model's results. A Y dimension width of 120 meters (roughly three times the building's longest dimension of 40 meters) was initially used based on the results of Kennedy and Duff's study *Blast Simulator Flow Blockage Control* (7:862). The Y dimension width of 150 meters was chosen after a series of runs were accomplished to determine the effect of flow restriction on the impulse received by the building. Figure 16 shows how the impulse decreases as the Y dimension width is increased, until errors from flow restriction are no longer affecting the impulse value.

*Resolution.* The mesh resolution was driven primarily by computational requirements. Computational time increased dramatically with increasing number of cells in the mesh for two reasons. Additional cells add to the number of computations required for each complete cycle through the mesh, and smaller cells require shorter time steps to keep the shock from moving a distance larger than one cell width each cycle. First gradually decreasing the X dimension cell size until 50 meters before the building's corner, keeping the cell size constant at 0.5 m for 50 meters, then gradually increasing the cell size in the outflow region worked well for the X dimension of the mesh. Attempting to gradually decrease then increase the cell size



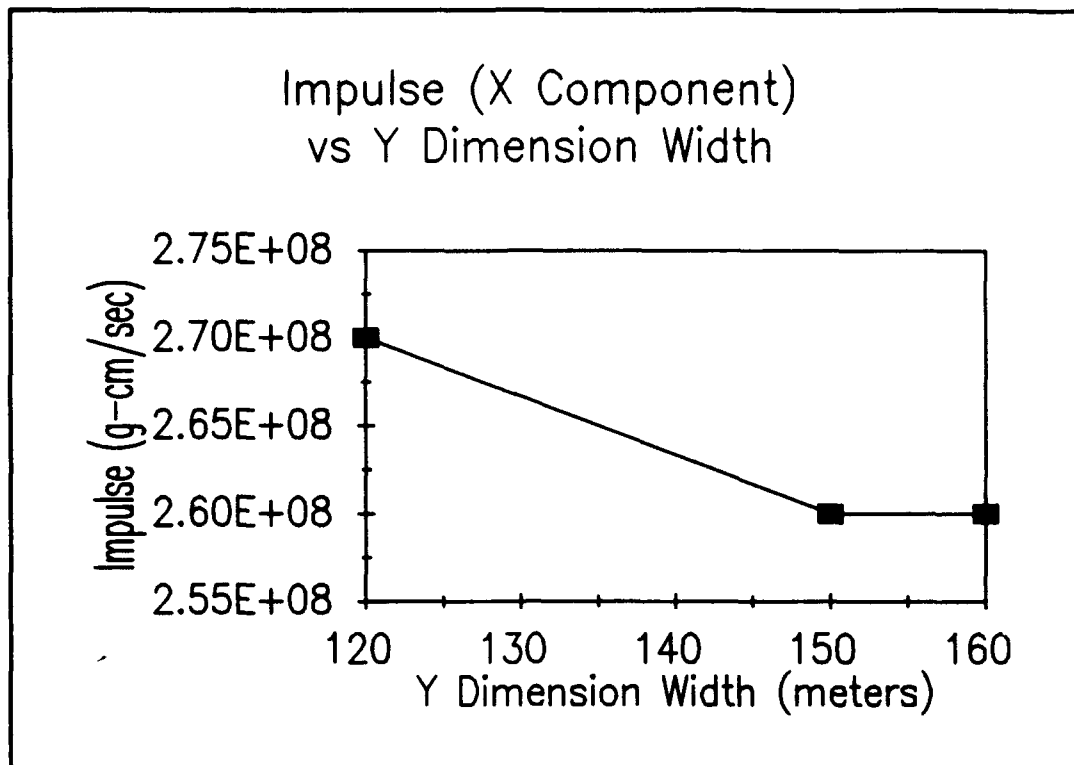


**Figure 16. Impulse (X Component) versus Y Dimension Width**

in the Y dimension introduced significant errors into the planar shock front caused by the changing aspect ratio of the cells. This forced the use of an evenly spaced Y dimension resolution of 0.5 meter per cell, coupled with the X dimension resolution gradually changing from 1 meter to 0.5 meter and then back to 1 meter. This achieved a 0.5 meter by 0.5 meter resolution in an impact area 50 meters wide between  $X = -50$  meters and  $X = 0$  meters. The number of cells used for the strong shock's mesh was 111,000 cells, and the weak shock used 161,400 cells.

*Boundary Conditions.* CTH provides three types of boundary conditions: totally reflective, sound speed based absorbing, and a pressure extrapolated boundary. The reflecting boundary was used for the left side (negative X direction) to simulate the center of a nuclear explosion. A sound speed based absorbing condition was used to allow the shock to flow out the right hand side of the mesh (positive X direction). Since the sound speed based absorbing condition approximates an infinite media, this boundary condition was originally chosen as a means to decrease the required Y dimension width without introducing flow restriction errors (3:B.2-2). Unfortunately, the edges of the planar shock front were absorbed as the shock propagated in the positive X direction, and the Y dimension boundaries had to be changed to reflecting boundaries. This required the Y dimension boundaries to be far enough from the building to reduce the effects of shocks reflecting off of the boundaries and striking the building. The pressure extrapolation boundary led to immediate dissipation of the shock, and was not further considered.

#### *Calibration of Code*

The two shock waves developed have many but not all of the characteristics of the ideal blast wave. The next step was to run models of these shocks striking a flat face (normal incidence) and see if the reflected overpressure and reflected impulse were comparable to compilations of theoretical and experimental data. Calibration models were developed using long rectangular buildings, arranged so the shock was normally incident on the short face. The long sides of the building prevent the shock

from reaching the rear of the building and equalizing the pressure before the negative phase has reached the front face (See Figure 17).

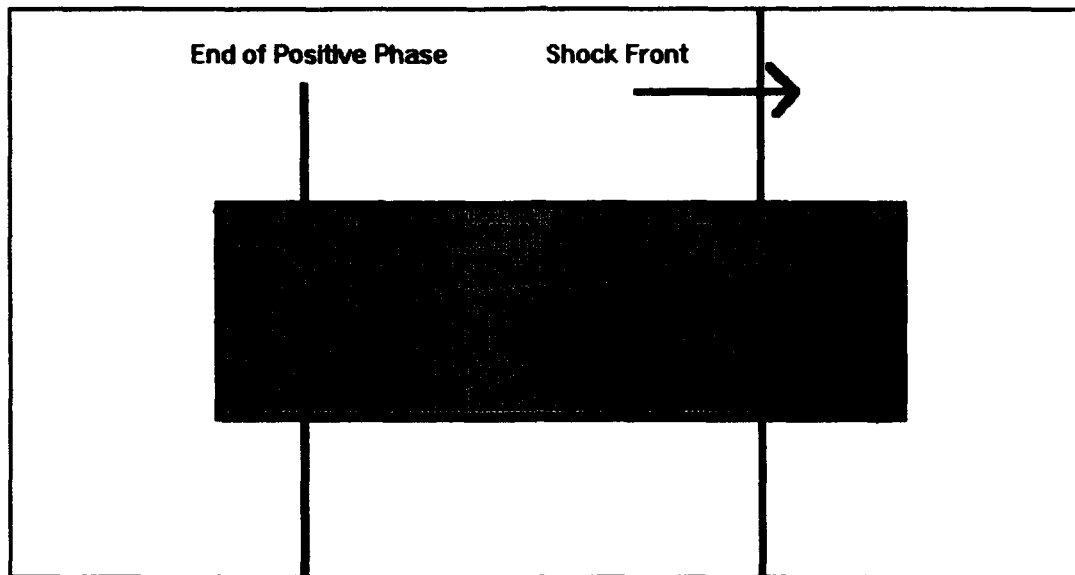


Figure 17. Long Rectangular Building Used for Code Calibration

*Overpressure Calibration.* The reflected overpressure for a normally incident shock wave striking a flat surface was computed using equation (11). For the 1.02 atmosphere overpressure shock wave, equation (11) predicts a reflected overpressure,  $p_r$ , of 2.82 atmospheres, and a reflected overpressure of 1.09 atmospheres for the 0.46 atmosphere overpressure shock wave. The values computed by CTH compare well to the predictions: reflected overpressure of 2.73 atmospheres for the higher overpressure shock, and reflected overpressure of 1.12 atmospheres for the lower overpressure shock. The differences between the values computed by CTH and the predicted values are approximately 3 percent.

*Impulse Calibration.* Impulse was computed by CTH on the basis that the change in momentum of a body acted on by an impulsive force is equal to the impulse received (6:155). CTH is able to compute the momentum of a block of material in a model from data in the history file. The peak momentum reached by the material is equal to the peak impulse received since the building was initially at rest. Using the two-dimensional rectangular geometry, CTH provides momentum data as if you were looking at a one centimeter tall slice of an infinitely tall building. Predicted values of the normally reflected positive impulse received by a 1 cm tall slice of a 40 meter wide building were computed from compiled impulse data in Baker's *Explosions in Air* (See Appendix C). Predicted impulse values were computed to be  $3.5 \times 10^8$  g-cm/sec for the higher overpressure shock and  $2.1 \times 10^8$  g-cm/sec for the lower overpressure shock (2:161). The impulse values computed by CTH were  $3.72 \times 10^8$  g-cm/sec and  $1.73 \times 10^8$  g-cm/sec for the higher and lower overpressure shocks respectively. The impulse predicted for the 0.46 atmosphere overpressure shock wave differed the greatest with a 18 percent difference, compared to the 1.02 atmosphere overpressure shock wave's difference of 6 percent.

### *Interaction With Structures*

The final step in the investigation was to run the shocks into the desired building shapes. This involved first modeling the buildings, then observing how the shock was interacting with the different structures to determine peak reflected overpressure and impulse received by each building. Therefore, there are two

possible ways to interpret the form of the shock front that is striking the buildings. Since the building is infinitely tall, one way is to view the shock - building interaction as a one kiloton free air burst blast wave striking the building at a height on the building equal to the height of burst of the weapon. The height of burst would be such that the shock is not reflecting off of the ground during the problem time, so only a single, nearly planar shock wave is striking the building. The second way to interpret the shock - building interaction modeled is as a 0.5 kiloton contact surface burst, where the shock wave near the ground is roughly planar. In this case, the slice of the building being modeled is at ground level. As discussed on page 21, the shock parameters of overpressure and positive phase duration are identical for these two scenarios.

*Modeling the Buildings.* The two-dimensional rectangular geometry chosen provided many options for modeling complex building shapes. The user defined shape (UDS) was used to model the L-shaped building as shown in Figure 1. This shape could then be rotated to any desired angle. For this investigation, models were done with the L-shaped building rotated 22.5, 45, 67.5, and 90 degrees counterclockwise from the original structure shown in Figure 1, as well as a model run with the building at zero degrees. Figure 18 shows these additional buildings used.

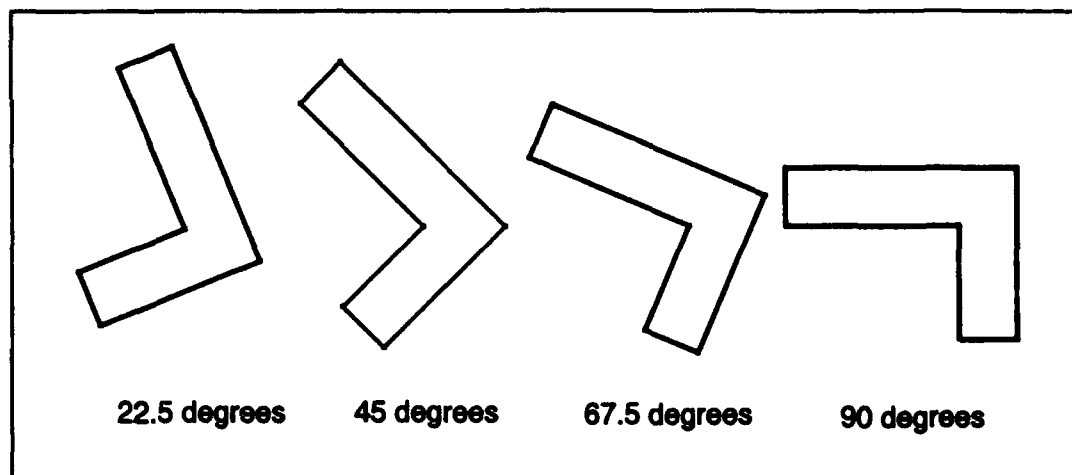


**Figure 18. Additional L-Shape Buildings**

For the atrium buildings, simple box shapes were used for the two wings. The two boxes were originally oriented with the long sides parallel to the X and Y axes respectively. Both wings were then rotated 45 degrees counterclockwise as a unit to create the structure shown in Figure 2.

All buildings were made of a material with the basic properties of iron, but with altered Mie-Grüneisen equation of state parameters. Previous work by Captain John Loftis showed that using steel as the building material allowed transmission of the shock deeply into the building. The high speed of the shock propagating through the steel building shortened the time step being used in the computation, and greatly lengthened computational times. Captain Grant Fondaw changed the building material to iron to enable use of the Mie-Grüneisen equation of state, then changed the sound speed parameter from  $4.572 \times 10^5$  cm/sec to 100 cm/sec. This change prevented the shock wave from propagating deeply into the building, and decreased problem run

times by approximately 60 percent because the shock's movement through the ambient air, which has a sound speed of  $3.4370 \times 10^4$  cm/sec, now controlled the time step. Although not a realistic building material, the material reflected the shock like other rigid materials, as was shown on page 42 in comparing the predicted value for the overpressure from the reflection of a normally incident shock to that computed by CTH. Because the buildings were modeled as solid blocks, any change in strength parameters due to the artificial material properties would have no affect on the overall model, as long as the material did not fracture and separate into pieces or significantly deform. Using the Mie-Grüneisen equation of state also allowed increasing the density of the iron from  $7.798 \text{ g/cm}^3$  to  $30 \text{ g/cm}^3$ . This change ensured the building would resist movement, although some movement was required in order to calculate the impulse from the increase in the building's momentum. The peak building velocity observed was 2.44 cm/sec, so even if the building were moving at that velocity for the entire positive phase duration of 0.174 seconds, the building would move only 0.4 cm. Actually, the building's velocity increased rapidly to a peak at the time the pressure loading on the front and rear faces of the building were equal, then decreased because the rear face loading was higher than the front face loading due to decay of the overpressure on the front face of the building. Therefore, the buildings moved less than 0.4 cm throughout the problem time frame. The buildings exposed to the lower overpressure shock received lower impulses, and moved even less, because the longer positive phase duration was balanced by the lower building velocity.

*Shock Reflections.* How the shock reflected from the wings of the buildings depended on the angle the incident shock front made with the building wall, as described on Page 20. The buildings rotated 22.5 and 67.5 degrees counterclockwise each had one wall that the shock was striking with an angle of incidence small enough that Mach reflection could occur. However, the distances traveled (20 and 30 meters) were so short that no Mach reflections were visible with a resolution limited to 0.5 meters. Reflections from the faces of the buildings rotated 0, 45, and 90 degrees were all regular reflections. The combination of the two regular reflections, each with an overpressure higher than the incident shock, provided peak reflected overpressures much higher than for a normally incident shock.

The investigation's most interesting shock pattern occurred in the atrium building where the wings were separated by 4.24 meters. The next series of figures uses pressure contours to show how the shock reflects from the building walls. (The legend is shown in Figure 19.) The views shown are closeups to better show the shock fronts interacting with the building's walls. Additional mesh areas in both the X and Y dimensions were used during the computation to reduce errors due to flow restriction.



L = 5.5 atmospheres	F = 2.5 atmospheres
K = 5.0 atmospheres	E = 2.0 atmospheres
J = 4.5 atmospheres	D = 1.5 atmospheres
I = 4.0 atmospheres	C = 1.001 atmospheres
H = 3.5 atmospheres	B = 0.98 atmospheres
G = 3.0 atmospheres	A = 0.5 atmospheres

**Figure 19. Legend for Pressure Contour Plots**

In the first frame (Figure 20) the incident shock is about to reach the point in the mesh ( $X = 0$ ) where the building's corner was located for the L-shaped building. The  $X=0$  line was chosen to be the place where the shock waves matched the one kiloton reference blast wave, and so was used as the common placement line for the two types of buildings. Two regular reflection shock fronts are observed behind the incident shock, with an angle of reflection of approximately 45 degrees. The overpressure behind the two reflected shock fronts is approximately 2.5 atmospheres, slightly greater than twice the 1.02 atmosphere incident overpressure.

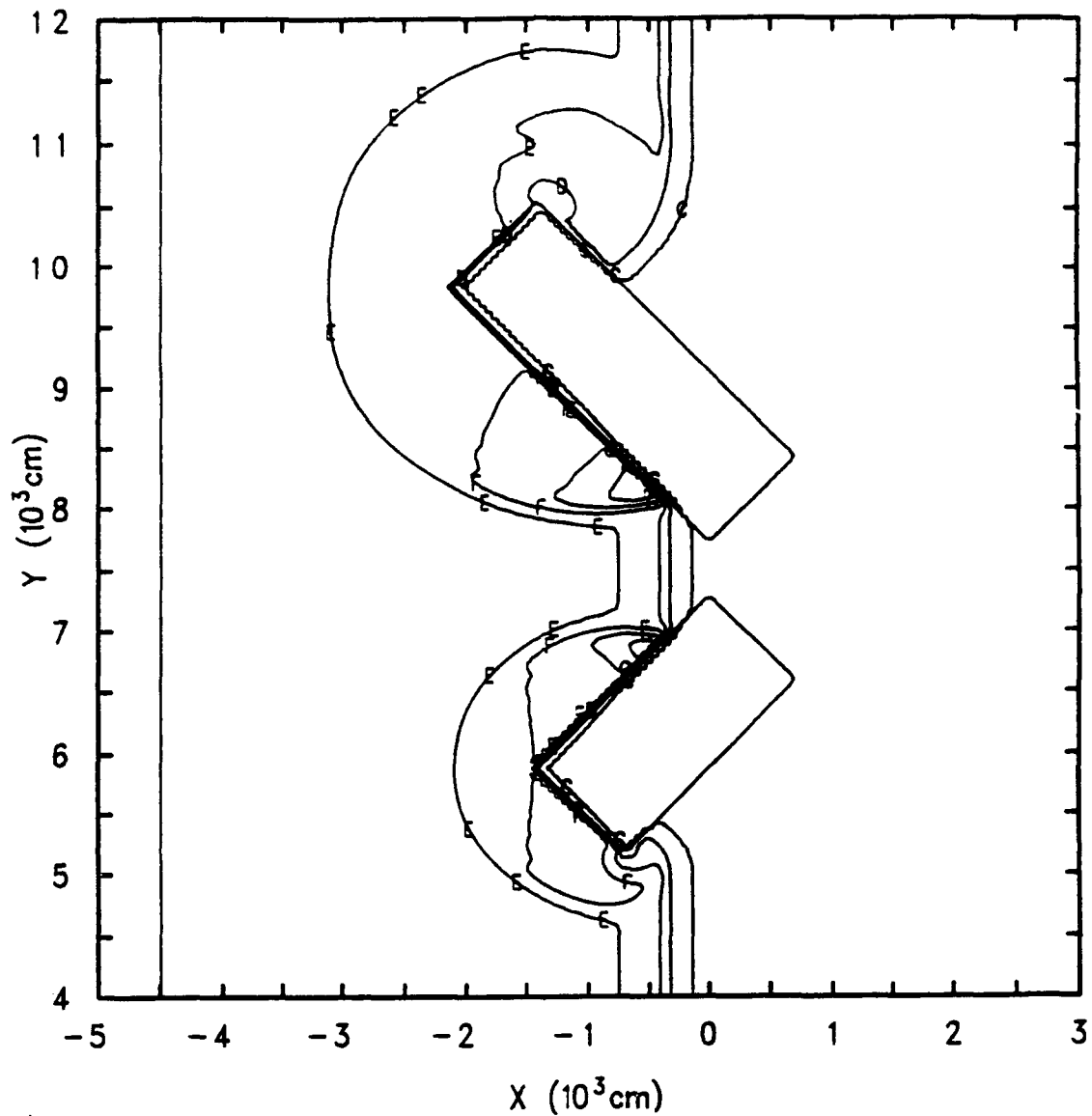


**Figure 20. Shock Striking Atrium Building, Frame 1**

In the next frame (Figure 21), the two reflected shock fronts are about to meet on the  $Y = 7500 \text{ cm}$  centerline between the two buildings. Because each reflected shock front is angled approximately 45 degrees from the incident shock front, the two reflected shock fronts are nearly parallel when they strike each other.

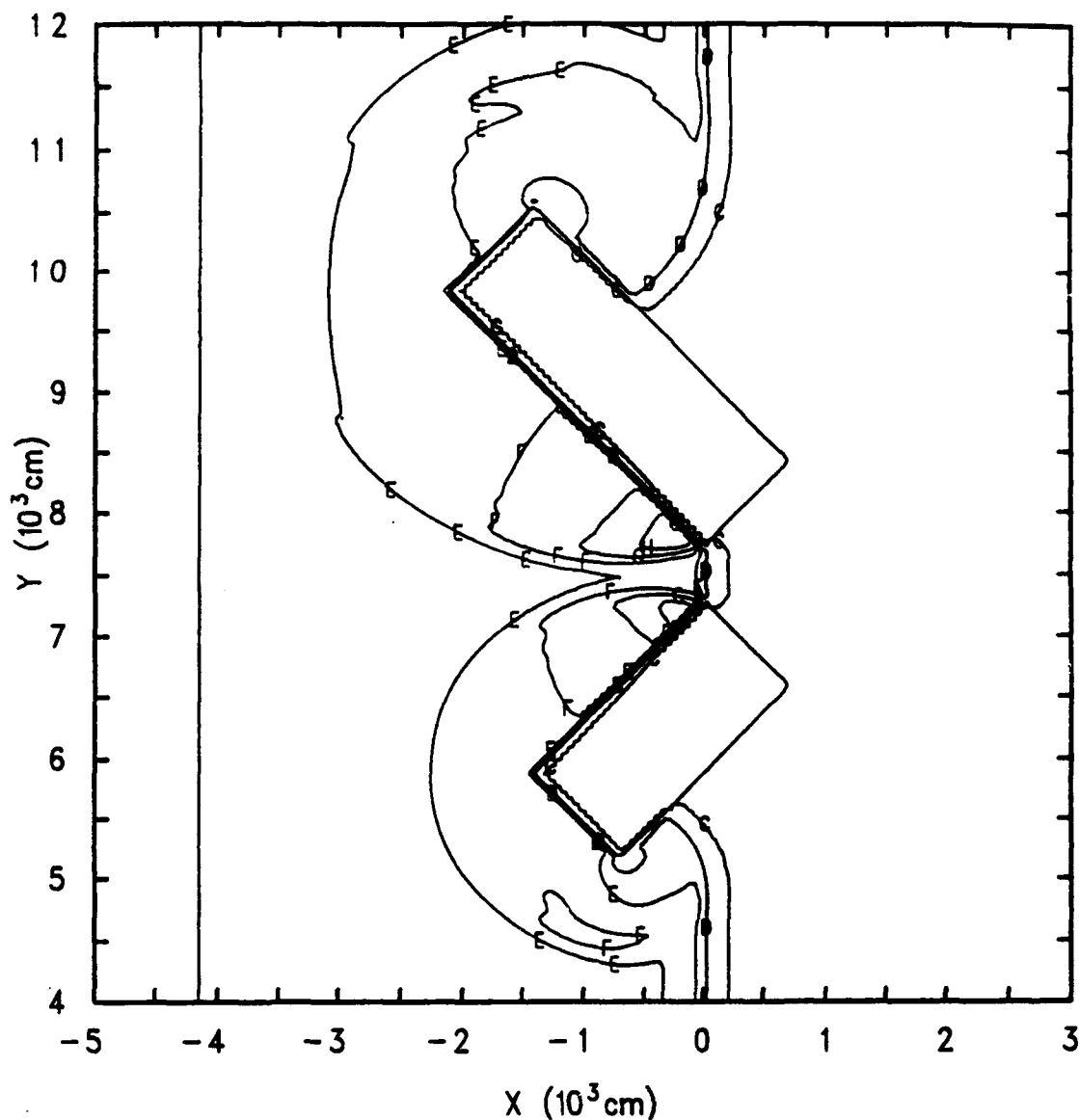


**Figure 21.** Shock Striking Atrium Building, Frame 2

In the third frame (Figure 22) the two reflected shock fronts have now struck each other with nearly normal (90 degree) incidence. Each shock experiences a overpressure increase due to the reflection as predicted by equation (11). This creates

an area of approximately 4.5 atmospheres overpressure on the  $Y = 7500$  cm centerline, slightly left of the  $X = 0$  impact zone.

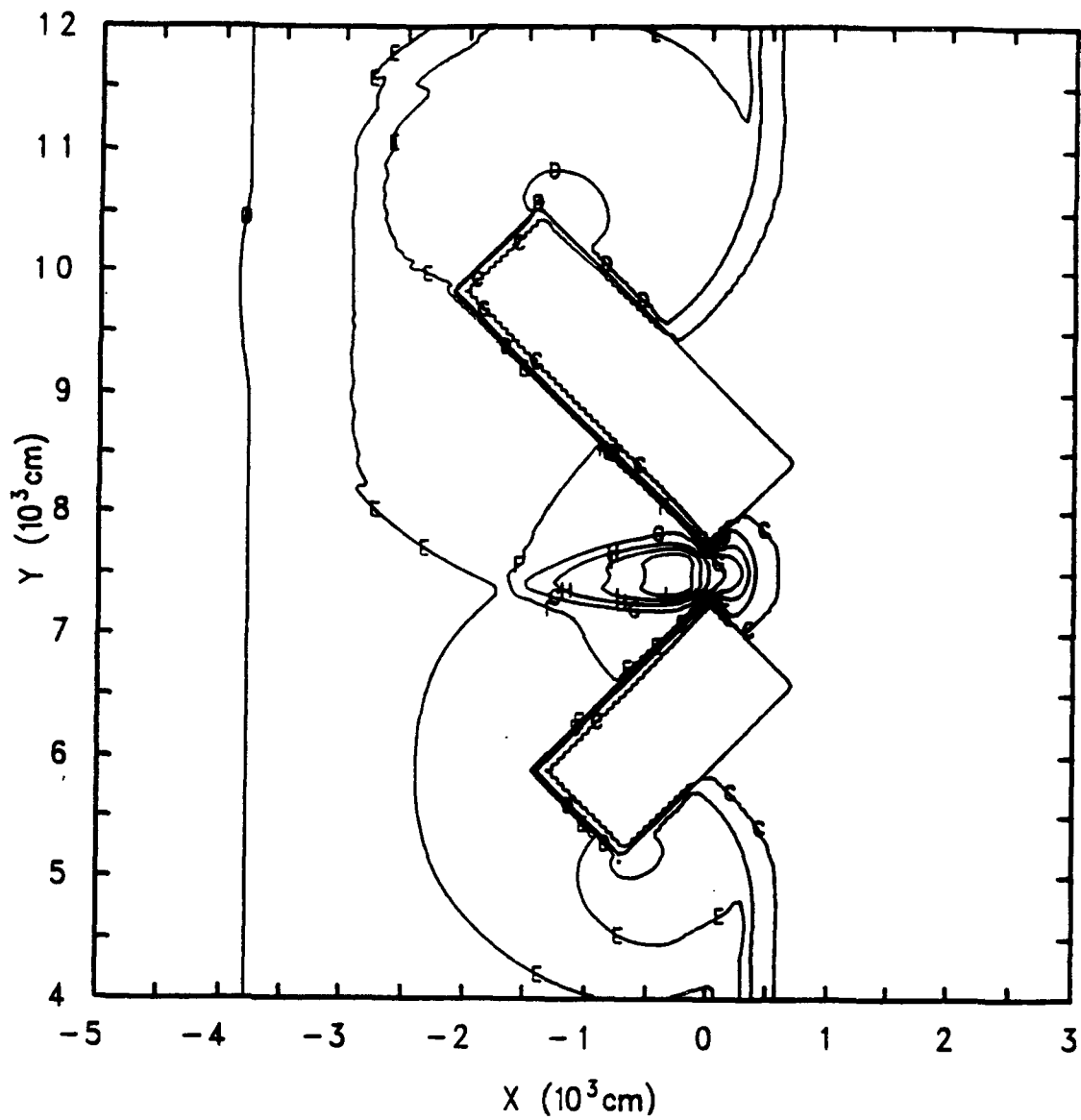


**Figure 22.** Shock Striking Atrium Building, Frame 3

Two new reflected shock fronts are formed from this collision on the  $Y = 7500$  cm centerline, which travel in the positive and negative  $Y$  directions until they strike the building walls with an angle of incidence of approximately 45 degrees (See Figure 23).

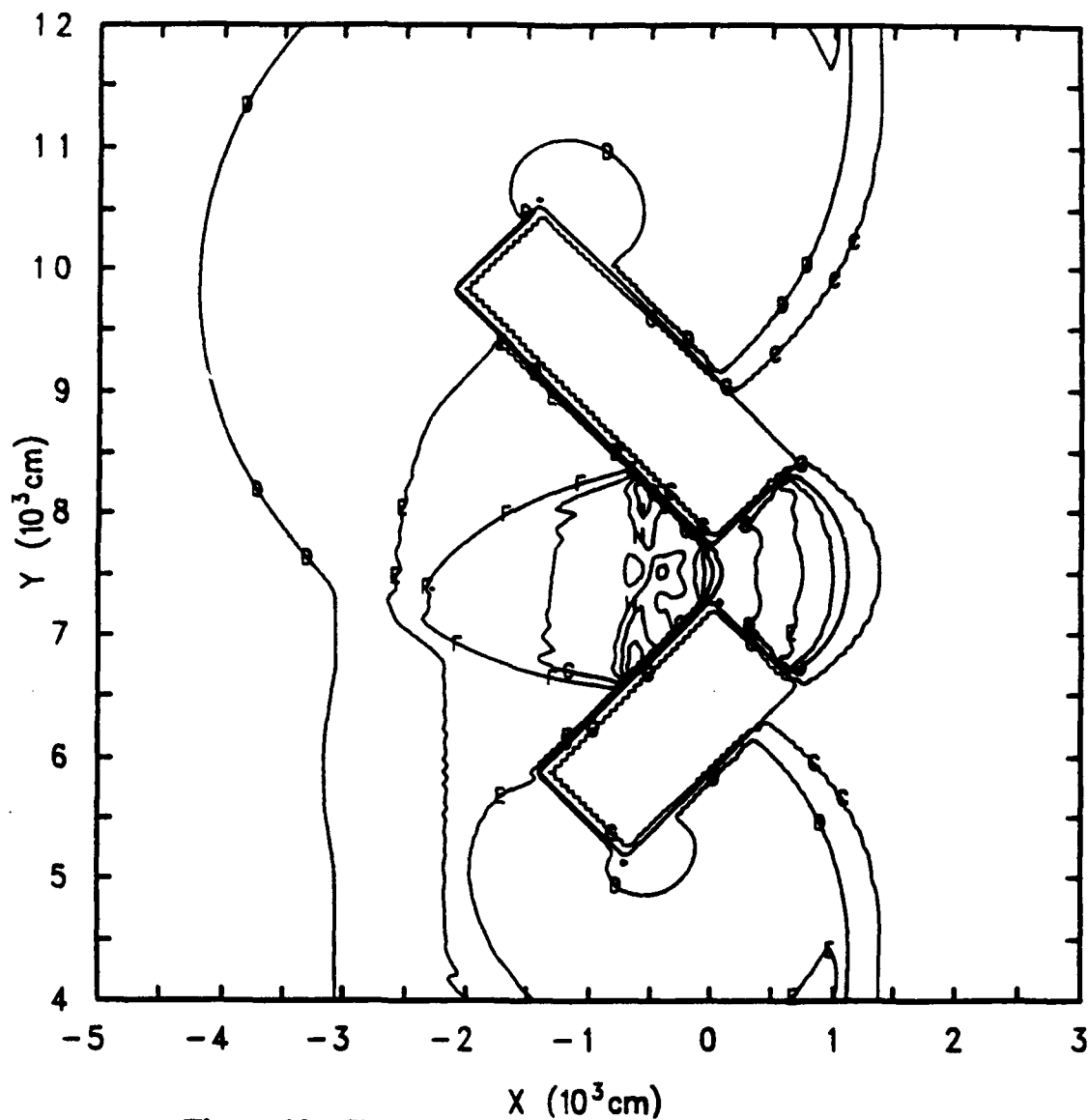


Figure 23. Shock Striking Atrium Building, Frame 4

It is this third set of reflections that produces the highest overpressure experienced by the walls. The shorter building wing receives the highest overpressure on its wall surface at approximately  $X = -3$  meters,  $Y = 72$  meters. The two shock waves that create this third set of reflections then travel out towards the large opening of the building (negative X direction), slowly dissipating in strength.

Shock flow patterns are similar for the L-shaped buildings, with the exception that the first set of two reflected shock fronts and the incident shock wave all meet nearly simultaneously in the corner, combining to achieve much higher overpressures than for the atrium buildings. Since the impulse on the building is linked to the peak overpressure by equation (10), the impulse was expected to be lower for the atrium buildings than for the comparable L-shaped building, as well as lower for the rotated L-shaped building angles that produced lower overpressures (See results on page 61).

Similar shock flow patterns result for the lower overpressure shock. The primary difference was in the magnitude of the increase in the reflected overpressure. Equation (11) predicts that stronger shocks will reflect with higher overpressures. This did occur, with the peak overpressure being 9.5 times the incident shock overpressure for the L-shaped building rotated 45 degrees exposed to the strong shock and only 6.9 times the incident shock overpressure for the same building exposed to the weaker shock.

#### IV. *Results*

Modeling shock - building interactions with CTH produces a tremendous amount of data (over 10 gigabytes for this investigation) because of the large restart files which represent the entire state of the model at the time the restart dump was written. The computational times involved in each model can be measured in hours, days, or weeks depending on the computer and geometry being used. Graphical interpretation helps in evaluating the data, but there are many aspects of the shock - building interaction models that are of interest. For this investigation, I chose to concentrate on two aspects of the interaction of shock waves with L-shaped structures: the peak reflected overpressures produced by the building shapes, and the impulses received by the building shapes during the overpressure positive phase duration.

##### *CTH Code Performance*

The CTH hydrodynamics code developed by Sandia National Laboratories works well in performing shock - building interaction analysis. After examining all available geometries, simulation of a Mach stem or the blast wave of a contact surface burst in two-dimensional rectangular geometry was chosen as the most appropriate model. Although assumptions concerning the building height and shock characteristics must be made, the two-dimensional rectangular model allows prediction of the reflected overpressure from L-shaped structures and a relative comparison of the impulse on the structures. Modeling the same shocks in three-dimensional

rectangular geometry would remove the infinite height building assumption, but would dramatically increase the computing costs required to meet the same resolution and flow restriction guidelines. For example, a building modeled in a 111,000 cell mesh in two-dimensional rectangular geometry would require 6,660,000 cells to be modeled as a 10 meter tall building in three-dimensional rectangular geometry. Two examples show the typical computing times involved in a two-dimensional rectangular model. Using the SUN workstations, a 111,000 cell mesh required 44.44 cpu hours. A nearly identical model, with only the building changing from L-shaped to an atrium building, required only 1.11 cpu hours on the Cray YMP at Los Alamos National Laboratories. Three-dimensional rectangular models would involve not just an increase in the number of cells, but the addition of complexity in the finite difference approximations of the conservation equations that would also increase computing time.

### *Reflected Overpressures*

The peak overpressure reflecting from the L-shaped building was significantly increased over that of a flat wall of equal surface area. This occurs because there are four shock fronts (one incident and one reflected for each wing of the building) that meet in the corner at approximately the same time and combine to produce a greatly increased overpressure. One model was run for each rotation angle: 0, 22.5, 45, 67.5, and 90 degrees. Table 3 shows how the reflected overpressure was lowest for the building set at 90 degrees, and highest for the building set at 45 degrees.



However, since only the five angles listed above were modeled, the actual peak overpressure could be produced at some other angle. As predicted by equation (11) the overpressure increase due to the corner is much higher for the stronger of the two shocks. Figure 24 shows the data graphically, however, please note that data was taken only at the rotation angles marked by squares and triangles: the building's asymmetric wings could cause the actual peak overpressure to be produced at some other angle not modeled.

Table 3

Reflected Overpressure, L-Shape Building		
	Incident Overpressure	
	1.02 Atmospheres	0.46 Atmospheres
Rotation Angle	Reflected Overpressure	Reflected Overpressure
(degrees)	(atmospheres)	(atmospheres)
0.0	2.91	1.21
22.5	5.38	2.31
45.0	9.73	3.16
67.5	5.49	2.44
90.0	2.88	1.19

Removal of the solid building material and placing an open courtyard (atrium) between the two building sections significantly reduced the peak overpressure on the building's walls. The L-shaped building rotated 45 degrees was used as the baseline

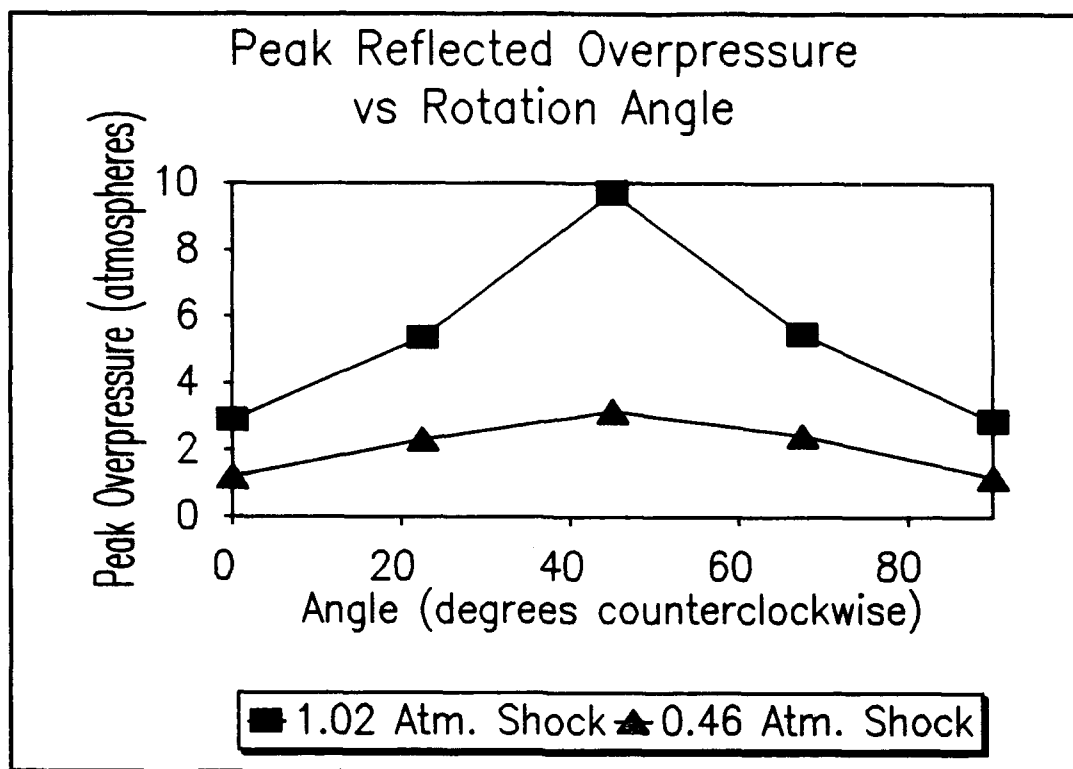


**Figure 24. Reflected Overpressure versus Rotation Angle, L-Shaped Building**

for the atrium buildings because it produced the highest reflected overpressure. By separating the building wings, the peak overpressure on the wall surfaces from the 1.02 atmosphere overpressure shock was reduced from 9.73 atmospheres to 4.86 atmospheres for the atrium building with a separation distance of 4.24 meters. Increasing the separation distance further decreased the overpressure, with the building face receiving an overpressure of 3.96 atmospheres for a separation distance of 7.07 meters. Table 4 compares the values of the L-shaped building with no separation to the other atrium buildings modeled for both shocks. Figure 25 shows graphically the decrease in overpressure as the gap between the buildings is widened.

Table 4

Peak Overpressure on Walls, Atrium Building		
	Incident Overpressure	
	1.02 Atmospheres	0.46 Atmospheres
Separation Distance	Reflected Overpressure	Reflected Overpressure
(meters)	(atmospheres)	(atmospheres)
0.0	9.73	3.16
4.24	4.86	1.94
7.07	3.96	1.72

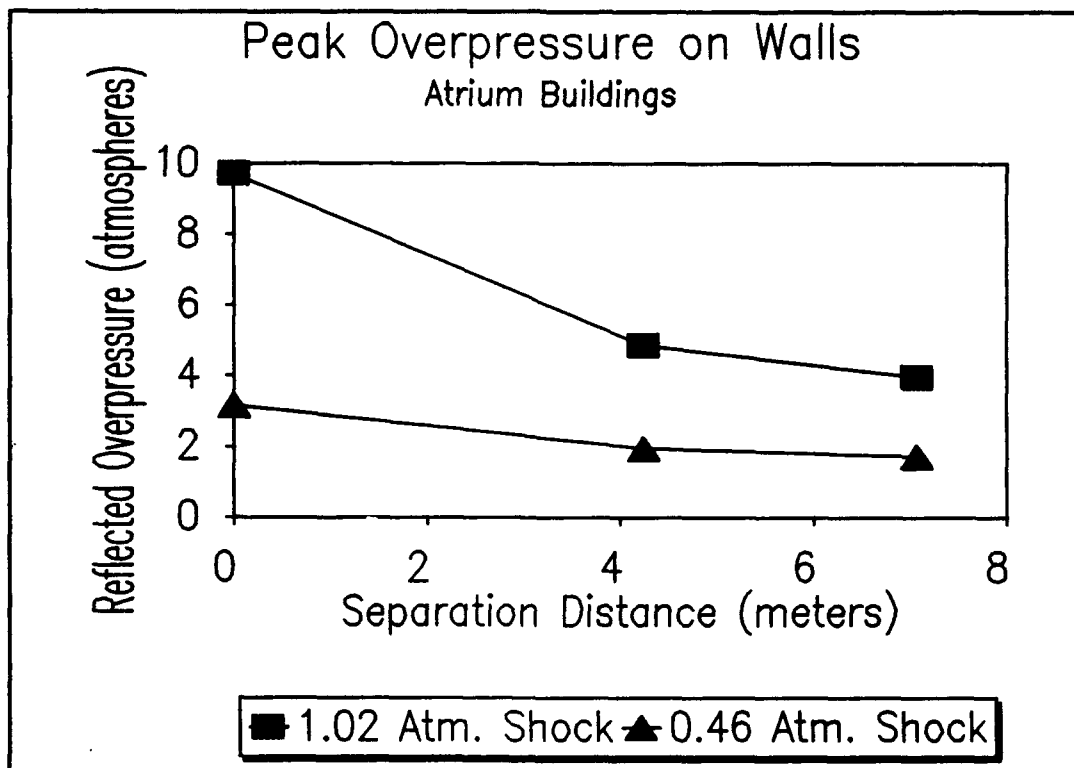


Figure 25. Peak Overpressure on Walls of Atrium Building

### *Impulse*

The impulse on the building is determined by the time history of the pressure on the building as shown in Equation (10). This dependence leads to higher values of impulse for the building rotation angles that led to higher overpressures. Again, the building rotated to 45 degrees experienced the highest impulse with a value of  $4.39 \times 10^8$  g-cm/sec for the higher pressure shock. Values for the impulse on the L-shaped building for both shocks versus rotation angle are listed in Table 5. The direction data shown in the table indicates the direction of the momentum vector for the building's center of mass. The zero degree direction is taken to be the positive X direction of the mesh. The building's momentum changes direction as the reflecting shocks load the different walls on the building, producing a twisting effect, even on the buildings at 0 and 90 degrees. The direction value given is the direction of the building's momentum vector at the time the peak momentum is observed. Figure 26 shows graphically how the highest impulse observed in this investigation was for the building modeled at 45 degrees, and lowest for the building modeled at 90 degrees. Again, the actual peak impulse could be at some rotation angle not modeled in this investigation.

Table 5

Impulse, L - Shape Building				
	Incident Overpressure			
	1.02 Atmospheres		0.46 Atmospheres	
Angle	Impulse	Direction	Impulse	Direction
(deg)	(g-cm/sec)	(deg)	(g-cm/sec)	(deg)
0.0	$3.92 \times 10^8$	-17.59	$1.78 \times 10^8$	-20.53
22.5	$4.34 \times 10^8$	-5.81	$2.06 \times 10^8$	-8.64
45.0	$4.39 \times 10^8$	8.53	$2.01 \times 10^8$	7.41
67.5	$3.59 \times 10^8$	21.53	$1.71 \times 10^8$	27.65
90.0	$2.67 \times 10^8$	25.9	$1.05 \times 10^8$	39.63

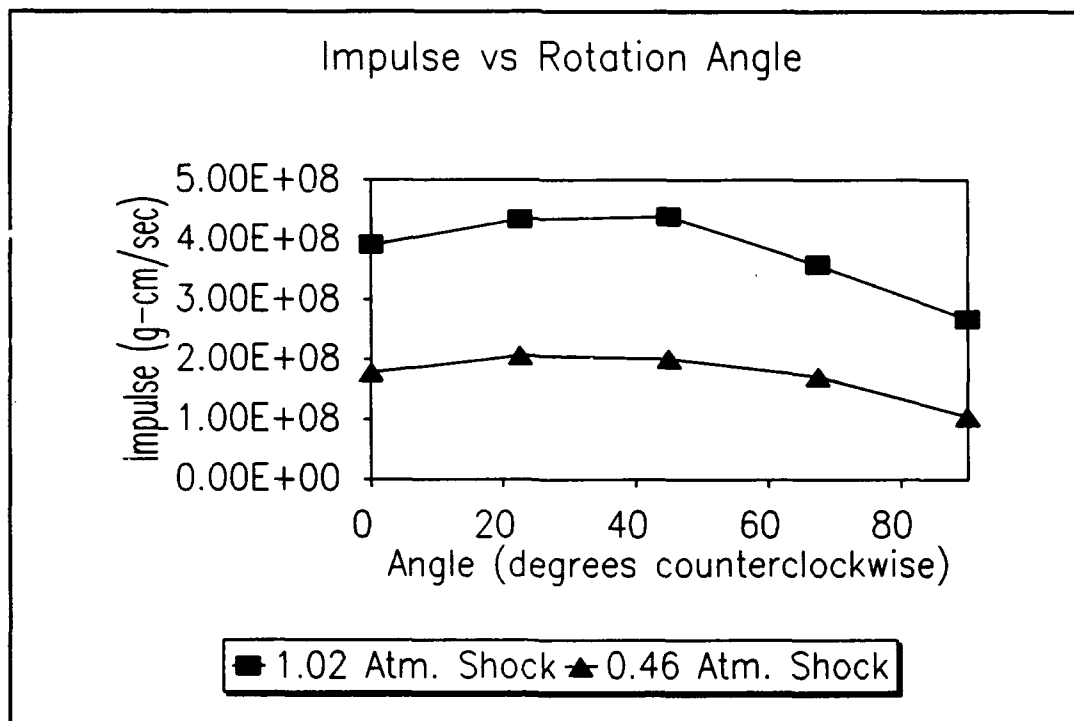


Figure 26. Impulse versus Rotation Angle, L-Shaped Building

The impulse on the atrium building was lower than for the joined building. This was expected since the relief passage of the atrium resulted in lower pressures pushing on the walls of the building. For the first separation distance, 4.24 meters, the impulse on the building was decreased by 15 percent from the value for the joined L-shaped building exposed to the higher overpressure shock. For the second separation distance, 7.07 meters, the impulse was decreased by 23 percent of the value for the L-shaped building struck by the 1.02 atmosphere overpressure shock wave. Table 6 shows the impulse values for the two separation distances and both shocks. The impulse on the atrium building struck by the lower overpressure shock unexpectedly increases as separation distance increases, even though the peak overpressure experienced by the building was lower. The two values would both round to a value of  $1.4 \times 10^8$  g-cm/sec, so it may be that numerical error is causing the unexpected increase in impulse. However, the error is more likely being caused by flow restriction, since separating the wings moved them out closer to the Y boundaries. Impulse values were more sensitive than overpressures to errors caused by flow restriction (See page 39). Figure 27 shows the change in impulse versus separation distance graphically.

Table 6

Impulse, Atrium Building				
	Incident Overpressure			
	1.02 Atmospheres		0.46 Atmospheres	
Separation Distance	Impulse	Direction	Impulse	Direction
(meters)	(g-cm/sec)	(degrees)	(g-cm/sec)	(degrees)
0.0	$4.39 \times 10^8$	8.53	$2.01 \times 10^8$	7.41
4.24	$3.71 \times 10^8$	8.25	$1.39 \times 10^8$	7.33
7.07	$3.39 \times 10^8$	9.21	$1.43 \times 10^8$	7.23

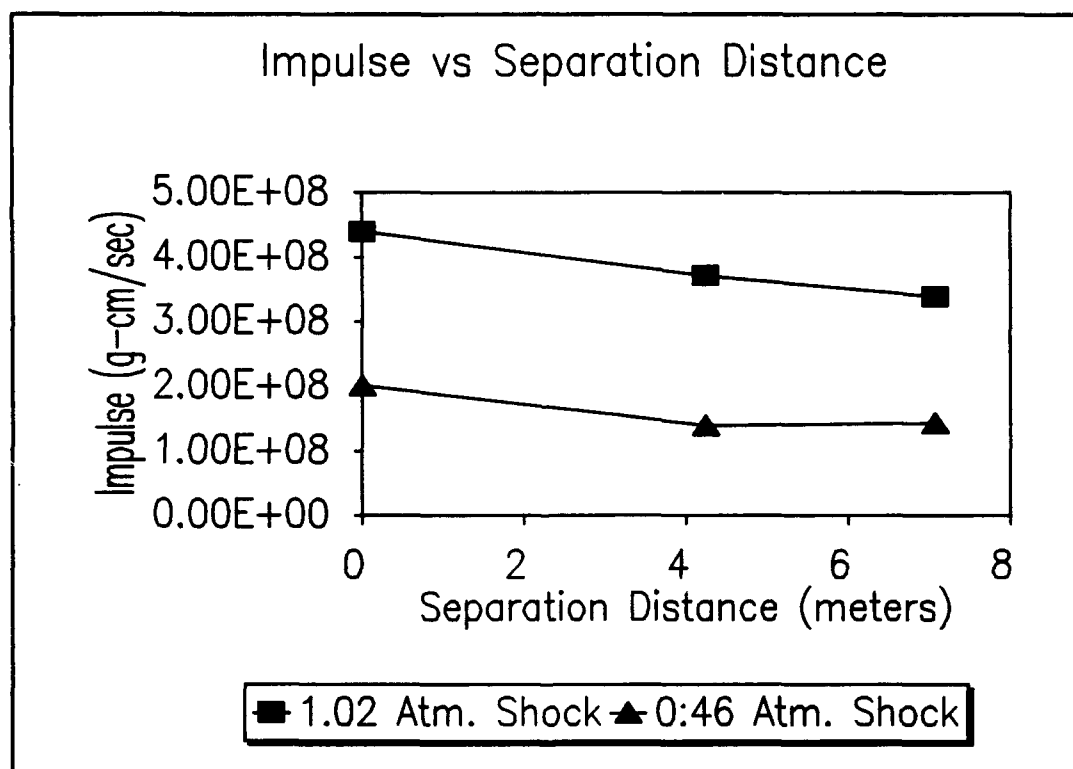


Figure 27. Impulse versus Separation Distance, Atrium Building

The decrease in impulse when an atrium is used as part of the building construction results in part because the blast wave can flow through the relief area. Equally significant is that the peak overpressure is no longer in the very corner of the building, but has moved out into the courtyard area between the buildings. The walls of the atrium buildings then receive a peak overpressure resulting from a reflection of the collision of the two shocks created by the original shock - wall reflections. This reflection reaches its peak overpressure approximately 3 meters from the corner of the 20 meter long wing (essentially the same location for both separation distances and shocks:  $X = -3$  meters,  $Y = 72$  meters), then travels back out of the courtyard in the negative X direction, rapidly decreasing in overpressure. This shift of the peak overpressure away from a corner and onto the flat wall of the building may reduce blast damage to the building.



## *V. Conclusions and Recommendations*

Sandia National Laboratories' CTH hydrodynamics code is both powerful and flexible. The code provides the tools to develop fairly strong shocks and model complex building shapes through combinations of its many shape options. Finally, CTH's developers provide many data output options, both graphical and numerical, to enable an analyst to view and interpret many different facets of a model. As such, CTH has significant potential for use in hydrodynamic modeling of both solids and fluids in a wide variety of problems useful to a weapons effects planner.

### *Conclusions*

This study showed that although the shock waves modeled by CTH were not perfect in all characteristics, peak overpressures computed by CTH matched predictions from shock theory within 3 percent. By matching the peak overpressure and positive phase duration of a CTH developed shock to the one kiloton reference blast wave at a specific distance, a nearly ideal blast wave was formed.

The shocks developed provided a useful tool for examining the peak reflected overpressure caused by the shock striking an L-shaped building at different rotation angles, and in comparing the impulse received by the buildings. I believe the impulse values are valid for comparison between the different rotation angles and building shapes, but do not represent an absolute value. Modeling the buildings in two-dimensional rectangular coordinates simulates an infinitely tall building. This

prevents the shock wave from passing over the building and equalizing the pressure on the rear face: instead, the shock wave must run around the building to reach the rear face. This source of error was minimized in the calibration models by using very long rectangular buildings, which keeps the shock from traveling over the building any faster than it would run down the sides to reach the rear face. This delayed the shock reaching the rear face of the building until the negative phase of the shock had reached the front face, allowing the impulse to build to the predicted value for a flat plate. Using this technique, values of the impulses predicted by the calibration models were within 18 percent of the predicted values (See Appendix C). However, I expect the values of the impulse calculated for the more complex shaped buildings to be higher than for a real blast wave on a three-dimensional building, because the shock acts longer on the building before pressure is equalized. The shock wave's inability to flow over the building has a lesser effect on the predicted overpressure, since the peak overpressure occurs almost immediately upon the incident shock wave striking the corner of the building.

Building a structure with an atrium joining the two wings at the corner provides a significant relief path to decrease the peak overpressure on the structure's walls. For the 1.02 atmosphere overpressure incident shock wave, the atrium building with a 4.24 meter separation distance experienced a 50 percent lower peak overpressure compared to a joined building at the same rotation angle. Decrease in the impulse received was less dramatic, with a 15 percent decrease for the same atrium building. The smaller reduction in impulse received by the building may

indicate that the largest percentage of the impulse is received as the incident shock travels down the walls of the building for the first time, prior to the shock wave reaching the impact zone. This part of the shock - building interaction is essentially the same for both the L-shaped and atrium buildings if the rotation angles are the same.

The two shocks modeled are fairly strong as far as survivability of even the most hardened buildings is concerned. According to Glasstone (5:219), a heavily reinforced building built to withstand 2 atmospheres of overpressure from a one megaton weapon would receive moderate damage for reflected overpressures of 3 atmospheres and severe damage for reflected overpressures of 4 atmospheres. The L-shaped and atrium buildings modeled in this study produced a wide range of reflected overpressures from 1.2 to 9.7 atmospheres. For the buildings exposed to the 1.02 atmosphere overpressure shock wave with a 45 degree angle of incidence, severe to total damage would be expected, even for the atrium buildings. The buildings exposed to the 0.46 atmosphere overpressure shock wave would have experienced damage in the light to moderate ranges. Glasstone defines the damage levels for a concrete reinforced blast resistant building as follows: light damage includes some cracking of concrete walls and frame; moderate damage is indicated by walls that are breached or nearly so, and extensive damage to building entrances; and severe damage includes shattered walls and a frame so distorted that collapse is imminent (5:214).

In summary, CTH was able to simulate shock waves realistic enough to predict reflected overpressures for a wide variety of building shapes or combinations of buildings. Comparisons of impulse received may also be done for building shapes exposed to the same shock wave. These comparisons, while not providing absolute impulse values, could be useful to weapons effects planners in designing shock relief paths or determining which building shapes shed a blast wave the best. Most importantly, CTH provides the capability to model groups of buildings as separate shapes, with relative impulse available for each building in the model.

### *Recommendations*

This investigation developed shock waves and buildings used to determine the peak overpressures created by shock reflections from L-shaped structures, and the positive phase impulses received by those structures. However, most of the investigation was accomplished in two-dimensional rectangular geometry, which places some limits on accuracy of the shock wave simulation. Initial attempts at creating shock waves in cylindrical and spherical geometries were promising, but much work will be required to develop techniques that will allow a shock developed in a non-cartesian geometry to propagate well in the two- and three-dimensional rectangular geometries CTH requires for structure modeling.

Shimming the walls of a rectangular mesh is a technique that could allow development of the shock wave in a one-dimensional cylindrical geometry that would propagate well once rezoned into a two-dimensional rectangular geometry. Triangular

shapes made of the same low sound speed material used for the buildings would be placed along the upper and lower Y boundaries of a rectangular mesh. The dimensions of each triangular shim would be determined by the need for the edge of the expanding cylindrical shock wave to be perpendicular to the hypotenuse of each triangular shim as shown in Figure 28.

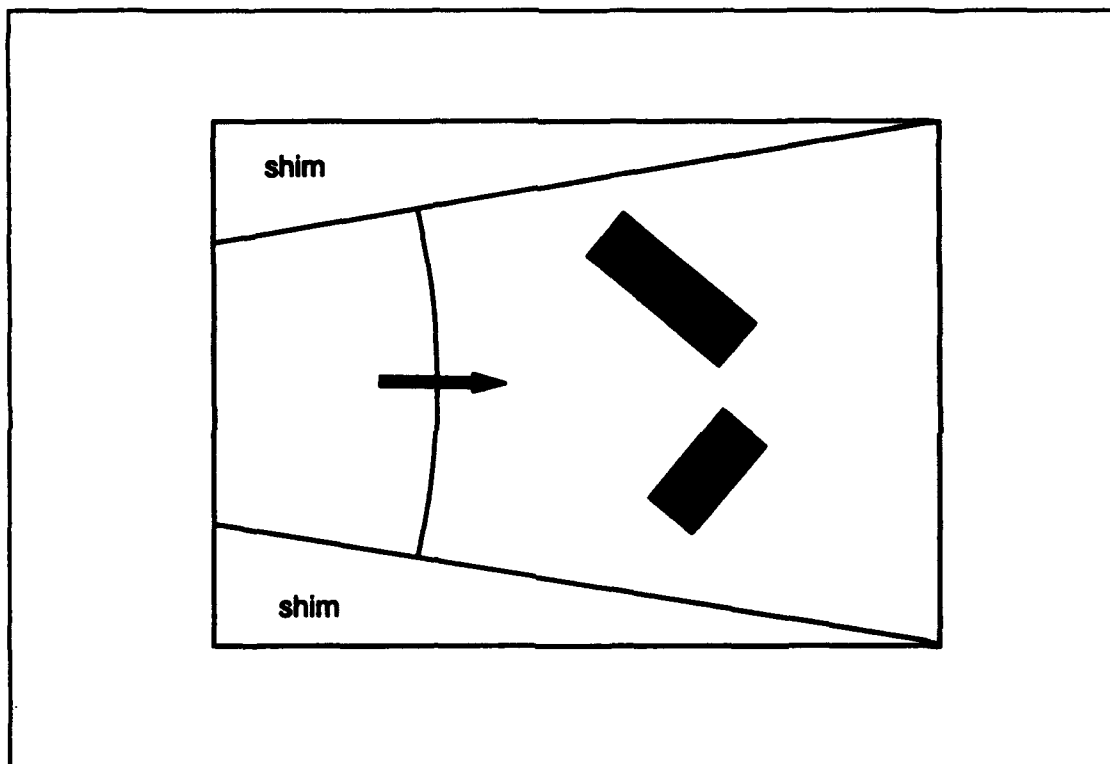


**Figure 28. Shimmed Wall Design**

A similar technique was used by Saillard, Barbry, and Mounier to transform planar shocks into cylindrical and spherical shocks through wall shaping (11:146). Shocks developed in a one-dimensional cylindrical geometry more closely approximate the

characteristics of the one kiloton reference blast wave over a wider range at the impact zone, which would help increase accuracy in analyses involving multiple buildings.

There are two areas involving three-dimensional rectangular geometry that merit further investigation as access to faster computers becomes available. First, extending the current two dimensional shocks into a three-dimensional planar shock could be done by making the compressed air region a three-dimensional box covering the Y - Z plane at the origin of the mesh. A shock developed this way should propagate through a three-dimensional rectangular mesh the same as it did in the two-dimensional rectangular mesh. The structures would have to be changed slightly, since the user defined shape (UDS) cannot have a height less than the full Z dimension width (3:A.9-17). Nevertheless, this technique would provide valuable information on impulse values when the shock wave is allowed to flow over the building. A second possibility to investigate involves developing a shock by inserting a spherically shaped compressed air region into a three-dimensional rectangular mesh, then running the model. Initial attempts with this technique showed promise, but the poor mesh resolution used to speed up computational times prevented any real conclusions being drawn about the potential for this technique. Again, access to faster computers should allow more timely exploration in this direction.

## Appendix A: Sample CTH Files

This first file is a stacked file that generates a mesh with both the shock and the building in it, runs the problem, then provides instructions for the history data plots and the contour graphics. The file sets up and runs the problem shown in the investigation section, in which the 1.02 atmosphere overpressure shock strikes the atrium building with a 4.24 meter separation distance between the wings.

```
*****
* atrium building in 15 psi shock for cray, gap = 4.24 meters
*
*****
*eor* genin
*
*****
* Title record
*
Shock generated by 6.3 atm in 800 cm
*
*****
* control records
*
control
  usessd
  mmp
endc
*
*****
* edit records
*
edit
  block 1
    expanded
  endb
ende
*
```

\*\*\*\*\*

\*

\* mesh records

\*

mesh

block 1 geom=2dr type=e

x0 -20000.

x1 w=12500 r=1 n=125

x2 w=2500 dxf=100 dxi=50

x3 w=5000 r=1 n=100

x4 w=2500 dxf=50 dxi=100

x5 w=7500 r=1 n=75

endx

y0 0

y1 w=15000 r=1 n=300

endy

xact -20000,-19200

endb

endm

\*

\*\*\*\*\*

\* material insertion records:

\*

insertion

block 1

\*

package compressed air

material 1

pressure 6.3e6

density 3.6981e-3

insert box

p1 -20000. 0.

p2 -19200. 15000.

endi

endp

\*

package steel

material 2

numsub 50

pressure 1.e6

insert box

p1 -2150,7350

p2 -150,6350



```

*
  ppoint 0,7500
  angle=45  *angle is rotation angle from y axis
*
    0, 22.5, 45, 67.5, 90
  endi
endp
*
package steel
  material 2
  numsub 50
  pressure 1.e6
  insert box
    p1 150,7650
    p2 1150,10650
*
  ppoint 0,7500
  angle=45  *angle is rotation angle from y axis
*
    0, 22.5, 45, 67.5, 90
  endi
endp
*
package an bient air
  material 1
  pressure 1.e6
  insert box
    p1 -19200. 0.
    p2 20000. 15000.
  endi
endp
*
  endb
endi
*
*****
*  tracer records (many tracer records removed for brevity)
*
tracer
  block 1
    add -975,8225 to 225,8225 n=25 fixed xy
  endb
endt
*
*****

```

```

* eos records
*
eos
  mat1 sesame eos=5031 feos='aneos' *air sesame
  mat2 MGRUN R0=30 CS=100 S=1.92 G0=1.69 CV=5.18E10
ende
*
*****
*
*eor* cthin
*
*****
* Title record
*
Shock generated by 6.3 atm in 800 cm
*
*****
*
* control records
*
control
  usessd
  tst 0.5
  rdu 1800.
endc
*
*****
*
* cell thermo records
*
cellthe
  mmp
endc
*
*****
*
* edit records
*
edit
  shortc
    cycle = 0 dc = 1000
  ends
  longt

```

```

    time = 0. dt = 1e5
endl
plott
    time = 0. dt = 2.5e-2
    time = 0.2 dt = 5e-3
    time = 0.3 dt = 2.5e-2
endp
histt
    time = 0. dt = 5e-4
    htracer all
endh
ende
*
*****
*
* boundary condition records
*
*****
*
boundary
    bhydro
        block 1
            bxb = 0 bxt = 1
        endb
    endh
endb
*
*****
*
*eor* hisin
*
units cgsev
*
plot time mat-x-mom.2 wrtout
plot time mat-mass.2
plot time mat-y-mom.2 wrtout
plot time pressure.148 wrtout
*
*****
*
*eor* pltin
*
*****

```

```
*
units cgsev
dump=1 ddump=1
limits x=-20000,10000
limits y=0,15000
bottom=off
MESH
noid
title='Shock Front Approaching Building'
CONTOURS=0.98e6, 1.001e6, 1.2e6, 1.4e6, 1.6e6, 1.8e6, 2.0e6
MCONTOURS=2.2e6, 2.4e6, 2.6e6, 2.8e6, 3.0e6, 3.2e6, 3.4e6
MCONTOURS=3.6e6, 3.8e6, 4.0e6, 4.2e6, 4.4e6, 4.6e6, 4.8e6, 5.0e6
MCONTOURS=5.2e6, 5.4e6, 5.6e6, 5.8e6, 6.0e6, 6.2e6, 6.4e6, 6.6e6
2D PLOT IF tracers CONTOURS=pressure
*
*****
```

Alternatively, a shock can be generated in a free field mesh, then rezoned to add a building and decrease the mesh width in the Y direction if necessary. The rezoned problem is then run and the data processed as above. The following file shows a stacked file which generates the 1.02 atmosphere overpressure shock wave, then provides the input deck to rezone the problem to add an L-shaped building rotated 45 degrees, and decrease the Y mesh width to 150 meters.

```
*****
*
* shock.2dr.x
*
*****
*
*eor* genin
*
*****
*
* Title record
*
Shock generated by 6.3 atm in 800 cm x 20000 cm
*
*****
*
* control records
*
control
  mmp
endc
*
*****
*
* edit records
*
edit
  block 1
    expanded
  endb
```

```

ende
*
*****
*
* mesh records
*
mesh
  block 1 geom=2dr type=e
    x0 -20000.
    x1 w=12500 r=1 n=125
    x2 w=2500 dxf=100 dxi=50
    x3 w=5000 r=1 n=100
    x4 w=2500 dxf=50 dxi=100
    x5 w=7500 r=1 n=75
  endx
  y0 0.
  y1 w=20000 r=1 n=200
  endy
  xact -20000.,-19200.
endb
endm
*
*****
*
* material insertion records:
*
insertion
  block 1
  *
    package compressed air
    material 1
    pressure 6.3e6
    density 3.6981e-3
    insert box
    p1 -20000.,0.
    p2 -19200.,20000.
    endi
  endp
  *
    package ambient air
    material 1
    pressure 1.e6
    insert box

```

```

        p1 -19200.,0.
        p2 10000.,20000.
    endi
endp
*
    endb
endi
*
*****
*
* eos records
*
eos
    mat1 sesame eos=5031 feos='aneos'          *air sesame
ende
*
*****
*
*eor* cthin
*
*****
*
* Title record
*
Shock generated by 6.3 atm in 800 cm x 20000 cm
*
*****
*
* tracer records (can add additional tracers here)
*
tracer
    block 1
        add -5025,10025 fixed xy
    endb
endt
*
*****
*
* control records
*
control
    tst 1.0
    rdu 1800.

```

```

endc
*
*****
*
* cell thermo records
*
cellthe
  mmp
endc
*
*****
*
* edit records
*
edit
  shortc
    cycle = 0 dc = 1000
  ends
  longt
    time = 0. dt = 1e5
  endl
  plott
    time = 0. dt = 5e-1
  endp
  histt
    time = 0. dt = 1e-4
    htracer all
  endh
ende
*
*****
*
* boundary condition records
*
*****
*
boundary
  bhydro
    block 1
      bxb = 0 bxt = 1
    endb
  endh
endb

```



```

*
*****
*
* rezl45.x
*
* Inserts l-shaped building with rotation angle 45
* degrees into mesh for 15 psi overpressure wave.
*****
*
*eor*rezin
*
*****
*
* Title record
*
rezone to include wall
*
*****
*
prerezone
  ofile='wave'    *shock wave in air
  file='rsctx'
  time=0.12
  numsub=50
  xmin=-20000
  xmax=-7500
*
  geometry
  mapping=2dto2d
    ce1=0,0
    ce2=0,250000 *no rotation
  endgeometry
*
endprerezone
*
*****
*
* control records
control
  time=0
  mmp
endc
*

```

```

*****
*
* edit records
*
edit
  block 1
    expanded
  endb
ende
*
*****
*
* mesh records
*
mesh
  block 1 geom=2dr type=e
    x0 -20000.
      x1 w=12500 n=125 r=1
      x2 w=2500 dxf=100 dxl=50
      x3 w=5000 n=100 r=1
      x4 w=2500 dxf=50 dxl=100
      x5 w=7500 n=75 r=1
    endx
    y0 0.
      y1 w=15000 r=1 n=300
    endy
    xact=-20000,-7500
  endb
endm
*
*****
*
* tracer records (many tracer records removed for brevity)
*
tracer
  block 1
    add -1075,7525 to 125,7525 n=25 fixed xy
  endb
endt
*
*****
*
rezone

```

```

file='wave'
endrezone
*
*****
*
* material insertion records
*
insertion
  block 1
    package steel
    material 2
    numsub 50
    pressure 1.e6
    insert uds
      p1 0,7500
      p2 0,10500
      p3 1000,10500
      p4 1000,6500
      p5 -2000,6500
      p6 -2000,7500
    *
    ppoint 0,7500
    angle=45      *angle is rotation angle from y axis
    *             0, 22.5, 45, 67.5, 90
    endi
    endp
  *
  package ambient air
  material 1
  pressure 1.e6
  insert box
    p1 -7500,0
    p2 10000,15000
  endi
  endp
*
endb
endi
*
*****
*
rezone
file='wave'

```

endrezone

\*

\*\*\*\*\*

\*

\* eos records

\*

eos

mat1 sesame eos=5031 feos='aneos' \*air sesame

mat2 MGRUN R0=30 CS=100 S=1.92 G0=1.69 CV=5.18E10

ende

\*

\*\*\*\*\*

## *Appendix B: Tips on Using CTH*

1. CTH generates a tremendous amount of data. The best way to look at results is graphically, but specific numbers can be generated too. The two basic graphic tools are CTHPLT and HISPLT. CTHPLT allows you to plot velocity arrows, contours, color contours, color bands, and many other types of graphical information.

CTHPLT obtains its values from the restart files, or from plot files if you used them. Over 50 variables are available for plotting, depending on the thermodynamic model used. The variables available are listed on page 10 of the CTHPLT User's Guide.

HISPLT allows the user to plot history data from tracers, as well as some global variables such as mass, volume, and momentum. Available HISPLT plot variables are listed on page F.2-1 of the CTH User's Manual. HISPLT is typically used to do X,Y type plots with time as the X variable. HISPLT also provides the opportunity to look at the actual numerical values through use of the WRTOUT command. For example, using the line "plot time pressure.34 wrtout" in a HISPLT input file will generate a time history plot of the pressure at tracer number 34, and write out the numerical data in two columns preceded by four header lines that identify the data.

Multiple PLOT and WRTOUT commands in a HISPLT input file will generate multiple plots, with each set of numerical data written to the file DATOUT in sequence. This DATOUT file can then be post processed using a spreadsheet or other program to find the peak value of the variable, combine two variables such as

using air velocity and density to determine the dynamic pressure, or perform any other desired computations.

2. HISPLT computes momentum for all the material of one type in a problem. If you are using more than one structure made of the same material in a problem, use the same equation of state parameters for each structure but name it a different material number. This will enable you to get the momentum separately for each structure. For example, if you have three iron buildings in a problem, call them materials 1, 2, and 3 in the material insert block, with corresponding entries in the equation of state block.

3. CTH numbers the tracer points in the sequence they are entered. A rezoned problem will retain its original tracer point numbers, even if the tracers are no longer within the problem boundaries. Adding tracers in the CTH run file can be done, but if the job is stopped and restarted, the tracers will be added again with new numbers, leading to multiple tracers at one location. Before using HISPLT, check the tracer numbers and locations in the orcth, ogcth, or octh file to ensure the plots desired will be done for the correct locations.

4. When using color plots from CTHPLT that will be viewed on both work stations and PCs, stick with the first eight colors of Color Table 2: black, red, green, yellow,

blue, purple, light blue, and white (numbers 0 - 7 respectively). The other colors tend to get confused in switching between the viewers POPX11 and POPVGA.

5. The sound speed based absorbing boundary condition was designed for use with solid materials. It will work as an outflow condition for the air shock problem, but should be kept fairly far away from the region of interest. The best approach for the other problem boundaries is to use the totally reflecting boundary condition, and keep the boundaries well away from the region of interest in the problem.

6. Restart and history files written by the Cray cannot be used by the SUN work stations, and vice versa. Graphics files and text files written by CTHPLT and HISPLT can be transferred and used on the different platforms. The graphics files must be transferred as binary files.

7. If you have disk space problems with a very large job, you can use CTHER to cut the last restart dump off of a restart file, copy the original file to tape, then rename the single restart dump to the original restart file name. This will enable you to restart where you left off, extending the same history file, but with a much smaller restart file.

8. Because CTH files can get so large, and problem run times so long (potentially weeks), you need to be aware of your disk space limitations and any scheduled system

down times. If the system crashes, or more typically runs out of disk space, you may lose all the data files associated with a problem. What gets lost depends very much on which files were open at the time of the crash, and what was in the system buffer. If you get lucky, you may be able to process the history and restart files up to the time of the crash, but you won't be able to continue the problem run. Use of CTH's backup restart option can help, as it writes alternating restart dumps to two separate files, one of which usually makes it through a crash. However, the best way to preserve intermediate data during a very long problem run is to stop the problem periodically and copy the history and restart files off to tape. This way, if the system crashes and all the files get ruined, you have clean files on the tape to restart from.



### *Appendix C: Calibration of Code*

Besides the normal benchmarking of a new code, results obtained from modeling the shock - building interactions with CTH needed to be compared to literature data for several reasons. First, the shocks used had only two characteristics that matched the one kiloton reference blast wave: overpressure and positive phase duration. Secondly, because the building material's equation of state parameters had been changed, I needed to determine if the shock waves were reflecting off of the buildings properly.

Although little work has been done with shocks interacting with complex shapes, there is a large amount of data available for shock waves reflecting off of flat plates, so modeling this interaction was used to determine the plausibility of the overpressures and impulses computed in my investigation.

The first step in calibrating the code was to determine if the overpressure produced by the planar shock front reflecting off of a flat surface would match the theoretical predictions. This was accomplished using equation (11), and is discussed in more detail on page 42. The fact that the overpressures produced from the newly developed shock waves striking models of flat plates agreed with the predicted values within 3 percent indicated that the unnatural building material was reflecting the shock as if it were a rigid surface, and was appropriate to be used for the remainder of the investigation.

The second part of the calibration of the code was to determine the reflected impulse when the shock waves reflected off of the flat plate model. I determined that using long rectangular building models would prevent the shock wave front from reaching the rear face of the building until after the shock's negative phase had reached the front face of the building (See Figure 17). Models were run of 40 meter wide by 140 meter long rectangular buildings for each of the two shocks, with resulting impulses of  $3.72 \times 10^8$  g-cm/sec for the 1.02 atmosphere overpressure shock and  $1.73 \times 10^8$  g-cm/sec for the 0.46 atmosphere overpressure shock.

Data from Wilfred E. Baker's *Explosions in Air* were used to calculate the predicted reflected impulses for the two shocks interacting with the 40 m wide rectangular buildings. Mr. Baker compiled experimental and theoretical airblast parameters from many sources including impulse data from analyses by C. N. Kingerly of the nuclear detonations Sugar, Fig, Little Feller I, Little Feller II, Johnie Boy, and Small Boy (2:130). Mr. Baker then scaled the available data and developed large (2.5 feet x 3 feet) graphs which are included in the back pocket of *Explosions in Air*. Using the following equations and Baker's Figure 6.3, Compiled Impulses and Durations, I computed predicted reflected impulses for the models of the two shock waves reflecting from a 40 meter wide flat surface.

First, I determined the scaled distance,  $\bar{R}$ , using the equation

$$\bar{R} = \frac{RP_0^{1/3}}{E^{1/3}}, \quad (13)$$

where  $P_0$  is the ambient air pressure and  $E$  is the energy released in the explosion.

Mr. Baker notes that the blast yield of a nuclear device was assumed to be only half the blast yield of TNT in preparing his compilations (2:126), so I used  $E$  equal to 0.5 kilotons energy in my calculations.

After the scaled distance was determined: 0.7665 for the 1.02 atmosphere overpressure shock wave and 1.095 for the 0.46 atmosphere overpressure shock wave, values of the side on (not reflected) scaled impulse,  $\bar{I}_s$ , were read from Baker's Figure 6.3 as 0.0395 for the 1.02 atmosphere overpressure shock wave and 0.0277 for the 0.46 atmosphere overpressure shock wave. The scaled reflected impulse,  $\bar{I}_R$ , was then calculated using

$$\bar{I}_R = \bar{I}_s \frac{P_R}{P_S}, \quad (14)$$

where  $P_R$  is the reflected overpressure and  $P_S$  is the incident overpressure.

Equation (14) is valid for scaled distances between 0 and 100 (2:160). Using values for  $P_R$  of 2.82 atmospheres and 1.09 atmospheres for the higher and lower overpressure shock waves respectively (values read from plots from the rectangular building CTH models), values for the scaled reflected impulses were 0.1092 for the 1.02 atmosphere overpressure shock wave and 0.0656 for the 0.46 atmosphere overpressure shock wave.

Finally, returning to the unscaled parameters using the equation

$$I_R = \frac{\bar{I}_R P_0^{2/3} E^{1/3}}{a_0}, \quad (15)$$

where  $a_0$  is the speed of sound in the ambient air (343.7 m/sec at 298 K), and multiplying by 4000 cm<sup>2</sup>, the surface area of the 1 cm tall slice of the 40 meter wide building as modeled by CTH in two-dimensional rectangular geometry gives values for  $I_R$ , the reflected impulse, of  $3.5 \times 10^8$  g-cm/sec for the 1.02 atmosphere overpressure shock wave and  $2.1 \times 10^8$  g-cm/sec for the 0.46 atmosphere overpressure shock wave.

## Bibliography

1. Anderson, John D. Jr. *Introduction to Flight*. New York: McGraw-Hill Book Company, 1978.
2. Baker, Wilfred E. *Explosions in Air*. Austin and London, University of Texas Press, 1973.
3. Bell, R. L., et al. *CTH User's Manual and Input Instructions*. Albuquerque, NM: Sandia National Laboratories, 1992.
4. Courant, R. and K. O Friedrichs. *Supersonic Flow and Shock Waves*. New York: Interscience Publishers, Inc., 1948.
5. Glasstone, Samuel and Philip J. Dolan. *The Effects of Nuclear Weapons (Third Edition)*. Washington: Government Printing Office, 1977.
6. Halliday, David and Robert Resnick. *Fundamentals of Physics*. New York: John Wiley & Sons, 1974.
7. Kennedy, Lynn W. and Russell E. Duff. "The Effects of Flow Blockage in a Blast Simulator and the Mitigation of these Effects with Flared and Vented Test Chambers" in *Shock Waves and Shock Tubes, Proceedings of the Fifteenth International Symposium on Shock Waves and Shock Tubes, Berkeley, California, July 28 - August 2, 1985*. Ed. Daniel Bershader and Ronald Hanson. Stanford, CA: Stanford University Press, 1986.
8. Kerley, Gerald I. *CTH Reference Manual: The Equation of State Package*. Albuquerque, NM: Sandia National Laboratories, 1991.
9. McGlaun, J. Michael. *CTH Reference Manual: Cell Thermodynamics*. Albuquerque, NM: Sandia National Laboratories, 1991.
10. McGlaun, J. Michael. *CTH Reference Manual: Lagrangian Step for Hydrodynamic Materials*. Albuquerque, NM: Sandia National Laboratories, 1990.
11. Saillard, Y., H. Barbry, and C. Mounier. "Transformation of a Plane Uniform Shock into Cylindrical or Spherical Uniform Shock by Wall Shaping" in *Shock Waves and Shock Tubes, Proceedings of the Fifteenth International Symposium on Shock Waves and Shock Tubes, Berkeley, California, July 28 - August 2, 1985*. Ed. Daniel Bershader and Ronald Hanson. Stanford, CA: Stanford University Press, 1986.

12. Air Force Systems Command Manual 500-8. *Effects of Airblast, Cratering, Ground Shock, and Radiation on Hardened Structures*. Washington, DC: Headquarters Air Force Systems Command, 1976.

### *Vita*

Richard Craig Miller was born on 1 July 1959 in Dayton, Ohio. He graduated from Appleton High School - East, Appleton, Wisconsin in 1977 and enlisted in the United States Air Force. In 1983, he received a Bachelor of Science degree in Chemical Engineering with High Honors from Michigan Technological University and was commissioned a Second Lieutenant in the United States Air Force. Upon graduation he was assigned as a Plans and Programs Manager at the Air Force Electronic Warfare Center, Kelly Air Force Base, Texas, where he earned a Master of Science in Systems Management from Saint Mary's University in 1986. In 1987, he completed the Cartographic and Geodetic Officer's Course as the Distinguished Graduate, and was promoted to Captain prior to being assigned to Defense Mapping Agency's Geodetic Survey Squadron, F.E. Warren Air Force Base, Wyoming. From 1989 to 1992, he served as the Commander, Detachment 4, Geodetic Survey Group at Patrick Air Force Base, Florida. He is currently assigned to the Air Force Institute of Technology, Wright Patterson Air Force Base, Ohio. He is a member of Tau Beta Pi and Phi Lambda Upsilon.

Permanent Address: San Antonio, Texas

REPORT DOCUMENTATION PAGE			Form Approved OMB No. 0704-0188	
Public reporting burden for this collection of information is estimated to average 1 hour per response, including the time for reviewing instructions, searching existing data sources, gathering and maintaining the data needed, and completing and reviewing the collection of information. Send comments regarding this burden estimate or any other aspect of this collection of information, including suggestions for reducing this burden, to Washington Headquarters Services, Directorate for Information Operations and Reports, 1215 Jefferson Davis Highway, Suite 1204, Arlington, VA 22202-4302, and to the Office of Management and Budget, Paperwork Reduction Project (0704-0188), Washington, DC 20503.				
1. AGENCY USE ONLY (Leave blank)		2. REPORT DATE December 1993		3. REPORT TYPE AND DATES COVERED Master's Thesis
4. TITLE AND SUBTITLE Shock Wave Interaction with L-Shaped Structures			5. FUNDING NUMBERS	
6. AUTHOR(S) Richard C. Miller, Captain, USAF				
7. PERFORMING ORGANIZATION NAME(S) AND ADDRESS(ES) Air Force Institute of Technology, WPAFB OH 45433-6583			8. PERFORMING ORGANIZATION REPORT NUMBER AFIT/GAP/ENP/93D-07	
9. SPONSORING/MONITORING AGENCY NAME(S) AND ADDRESS(ES) Lt Col Mark Byers DNA/SPWE 6801 Telegraph Road Alexandria, VA 22310-3398			10. SPONSORING/MONITORING AGENCY REPORT NUMBER	
11. SUPPLEMENTARY NOTES				
12a. DISTRIBUTION/AVAILABILITY STATEMENT  Approved for public release; distribution unlimited			12b. DISTRIBUTION CODE	
13. ABSTRACT (Maximum 200 words)  This study investigated the interaction of shock waves with L-shaped structures using the CTH hydrodynamics code developed by Sandia National Laboratories. Computer models of shock waves traveling through air were developed using techniques similar to shock tube experiments. Models of L-shaped buildings were used to determine overpressures achieved by the reflecting shock versus angle of incidence of the shock front.  An L-shaped building model rotated 45 degrees to the planar shock front produced the highest reflected overpressure of 9.73 atmospheres in the corner joining the two wings, a value 9.5 times the incident overpressure of 1.02 atmospheres. The same L-shaped building was modeled with the two wings separated by 4.24 meters to simulate an open courtyard. This open area provided a relief path for the incident shock wave, creating a peak overpressure of only 4.86 atmospheres on the building's wall surfaces from the same 1.02 atmosphere overpressure incident shock wave.				
14. SUBJECT TERMS  Air Shock, Shock Waves, Shock Wave Interactions			15. NUMBER OF PAGES 102	
			16. PRICE CODE	
17. SECURITY CLASSIFICATION OF REPORT Unclassified	18. SECURITY CLASSIFICATION OF THIS PAGE Unclassified	19. SECURITY CLASSIFICATION OF ABSTRACT Unclassified	20. LIMITATION OF ABSTRACT UL	